US Army Corps of Engineers
Waterways Experiment Station

Final Report
CPAR-SL-98-2
June 1998

CONSTRUCTION PRODUCTIVITY ADVANCEMENT RESEARCH (CPAR) PROGRAM

A Portable, Nondestructive Evaluation System

by

Fu-Chiarng Chen, Weng Cho Chew, A. Michel Alexander

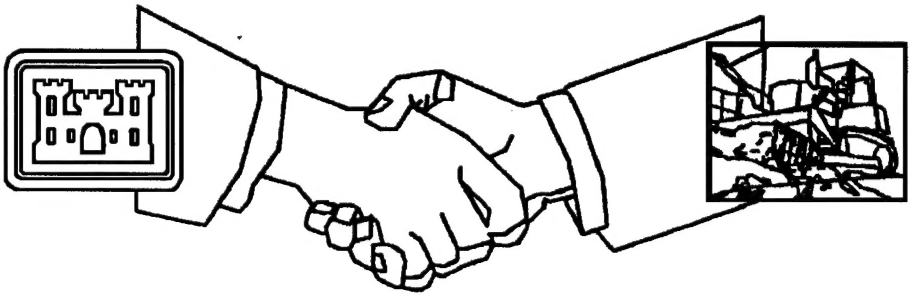

A Corps/Industry Partnership to Advance Construction Productivity and Reduce Costs

The contents of this report are not to be used for advertising, publication, or promotional purposes. Citation of trade names does not constitute an official endorsement or approval of the use of such commercial products.

The findings of this report are not to be construed as an official Department of the Army position, unless so designated by other authorized documents.

PRINTED ON RECYCLED PAPER

Construction Productivity Advancement Research (CPAR) Program

Technical Report
CPAR-SL-98-2
June 1998

A Portable, Nondestructive Evaluation System

by Fu-Chiarng Chen, Weng Cho Chew

Department of Electrical and Computer Engineering
University of Illinois
1406 West Green
Urbana, IL 61801

A. Michel Alexander

U.S. Army Corps of Engineers
Waterways Experiment Station
3909 Halls Ferry Road
Vicksburg, MS 39180-6199

Final report

Prepared for U.S. Army Corps of Engineers
Washington, DC 20314-1000

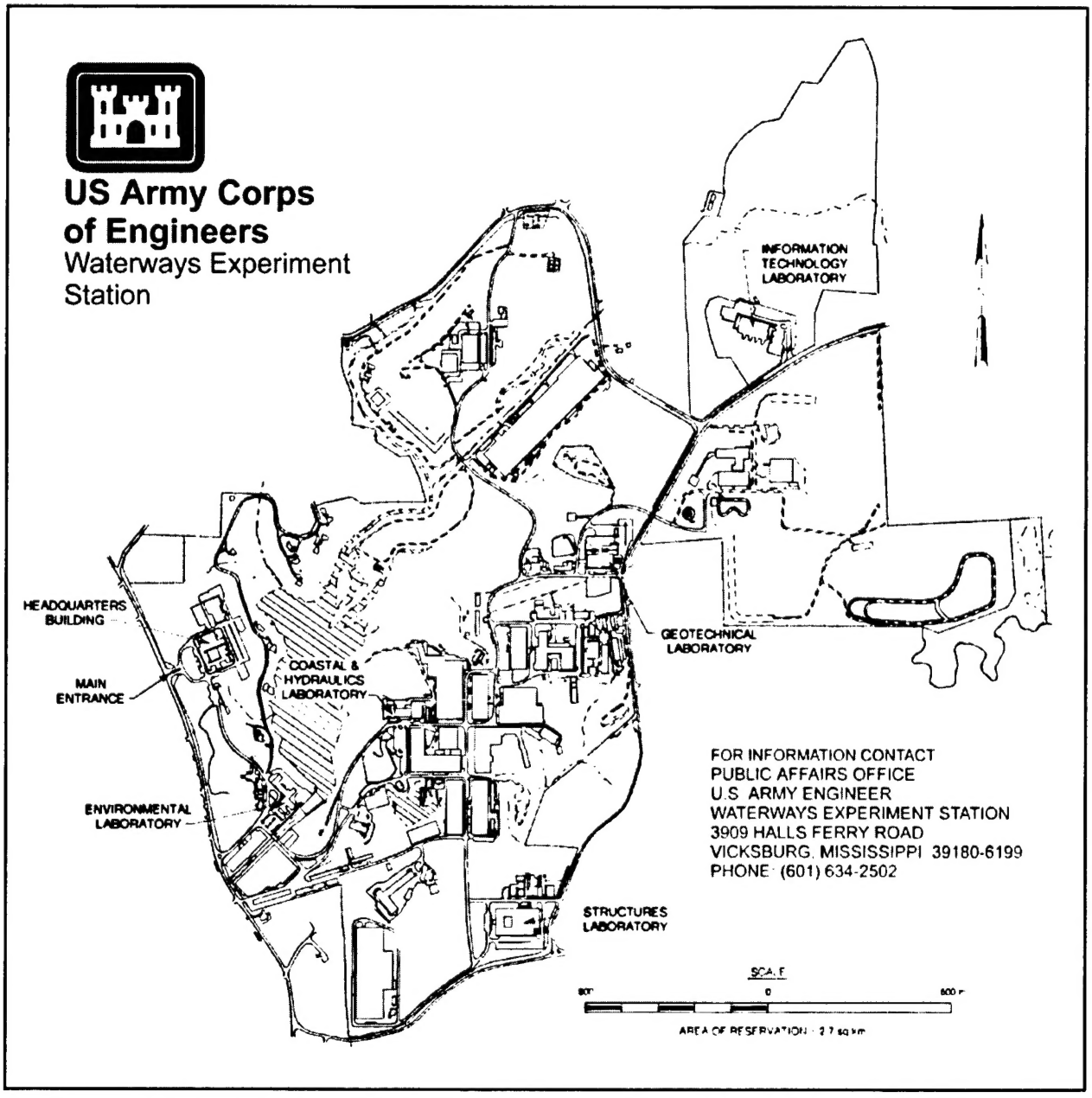

Waterways Experiment Station Cataloging-In-Publication Data

Chen, Fu-Chiarng.

A portable, nondestructive evaluation system / by Fu-Chiarng Chen, Weng Cho Chew, A. Michel Alexander ; prepared for U.S. Army Corps of Engineers.

57 p. : ill. ; 28 cm. — (Technical report ; CPAR-SL-98-2)

Includes bibliographical references.

1. Radar — Technique. 2. Non-destructive testing. 3. Concrete — Testing. I. Chew, Weng Cho. II. Alexander, A. Michel. III. United States. Army. Corps of Engineers. IV. U.S. Army Engineer Waterways Experiment Station. V. Structures Laboratory (U.S. Army Engineer Waterways Experiment Station) VI. Construction Productivity Advancement Research Program (U.S.) VII. Title. VIII. Series: Technical report (U.S. Army Engineer Waterways Experiment Station) ; CPAR-SL-98-2.

TA7 W34 no.CPAR-SL-98-2

Contents

Preface

The investigation described in this report was conducted for Headquarters, U.S. Army Corps of Engineers (HQUSACE), by the U.S. Army Engineer Waterways Experiment Station (WES), in collaboration with the Department of Electrical and Computer Engineering, University of Illinois, Urbana, IL. This cooperative research and development agreement was a part of the Construction Productivity Advancement Research (CPAR) Program. The HQUSACE Technical Monitors were Messrs. B. James, M.K. Lee, J. Foster, and D. Chen.

In enacting the Water Resources Development Act (WRDA) of 1988, Congress authorized the U.S. Army Corps of Engineers (USACE) to enter its laboratories and research centers into collaborative research/development with non-Federal entities on a cost-shared basis. As a result of the WRDA authorization, USACE initiated the CPAR Program in 1989. This Program provided funding for USACE Laboratories to enter into CPAR Cooperative Research and Development Agreements with non-Federal corporations, sole proprietorships, trade associations, state and local governments, and colleges/ universities, for the purpose of improving the productivity of the U.S. construction industry. USACE projects benefit from the use of CPAR technologies that result in improved construction productivity.

The purpose of this project was to develop a portable radar system for nondestructive evaluations (NDE) of concrete. An ultra-wideband time-domain pulse radar NDE system was developed at the University of Illinois under the supervision of Messrs. Fu-Chiarng Chen and Weng Cho Chew. Field testing was conducted at WES under the general supervision of Messrs. Bryant Mather, Director, SL; John Ehrgott, Assistant Director, Structures Laboratory (SL); William F. McCleese, CPAR Point of Contact at WES; and Dr. Paul Mlakar, Chief, Concrete and Materials Division (CMD), SL. Mr. A. Michel Alexander, CMD, was the Principal Investigator of this work unit. This report was prepared by Messrs. Chen, Chew, and Alexander.

At the time of publication of this report, Director of WES was Dr. Robert W. Whalin. Commander was COL Robin R. Cababa, EN.

1 Introduction

Background

Numerous nondestructive testing/nondestructive evaluation (NDT/NDE) methods and types of equipment are used to diagnose the condition of concrete in various civil structures: wave techniques such as radar, ultrasonic pulse velocity, impact-echo, thermography, etc., and various mechanical techniques such as Schmidt rebound hammer, Windsor probe, break off, pull out, etc. The major benefit of radar is its high speed of data acquisition. Electromagnetic energy travels at the speed of light and measurements can be made over a concrete surface in miles per hour as opposed to feet per minute or similar units, such as for acoustic-type systems. Speed is especially important for structures such as pavements but not as critical for Corps structures such as locks and dams.

Commercial radar units used for concrete were systems originally designed to detect the presence of tunnels through a few feet of soil from the ground surface in Vietnam; hence, the name ground-penetrating radar (GPR). However, there is a need to specifically design a radar unit around the mechanical and electrical properties of concrete rather than soil. Currently, a typical radar unit operating at a frequency that will give the best resolution for concrete can only penetrate to a depth of about 0.5 m (1.5 ft) in concrete. Lock and dam structures used by the Corps of Engineers have dimensions that far exceed this value.

Cost-effective maintenance decisions can be made from NDE surveys, which enable managers to set adequate budgets and plan for future maintenance, rehabilitation, or replacement needs. The cost of NDE assessment is always an important consideration for Corps of Engineer Districts that are responsible for operation of their structures.

GPR has been used to obtain information for the following types of problems relating to concrete structures:

a. Moisture accumulation in deteriorated areas.

b. Chloride content of concrete.

c. Corrosion of reinforcing steel.

d. Concrete cover over reinforcement, position, and amount of steel reinforcement.

e. Internal cracking.

f. Lack of consolidation (honeycombing).

g. Foreign objects.

h. Delaminations in bridge decks.

i. Voids beneath concrete foundations.

j. Thickness of layer.[1]

The construction industry is long overdue for improved diagnostic techniques to evaluate the condition or quality of concrete. New and improved NDT systems will permit a better evaluation of the quality of construction and the condition of older structures. They will reduce the dependence on drilling cores and the attendant high cost to determine the structure's integrity. The esthetics of the structures will benefit, as reduced surface marring will take place from limited coring. Also, better NDT systems should result in prompt, improved information about the condition of the structure so that preventive maintenance can be performed before the structure has reached the post-mortem stage. Ideally, the data should be processed in real-time and onsite for early feedback and processed off-line at the laboratory for improved resolution.

In summary, better NDT units will afford faster evaluation of structures, more thorough evaluations, cost savings, and will permit managers of structures to better schedule an ongoing program of cost-effective maintenance and rehabilitation. Because NDT is a specialized service requiring experts skilled in various disciplines, including civil engineering, it is customary for the construction industry to hire firms that provide NDT evaluation services rather than purchase the equipment themselves and attempt their own diagnoses. Customers that are made aware of the improved technology will require that firms purchase the new technology if they intend to remain competitive.

Objective

The objective of this work was to develop, test, and commercialize a new radar system specifically designed for the nondestructive evaluation of concrete structures. Presently, the construction industry uses GPR units to diagnose the condition of concrete.

---

[1] A. Michel Alexander, "Problems encountered and role for ground penetrating radar in concrete technology and Corps structures assessment." *Proceedings of the Government Users Workshop on Ground Penetrating Radar Applications and Equipment*, 26-27 March 1992, Vicksburg, MS.

Approach

The objective was to be met by conducting the following tasks: (a) design an array of receiving and transmitting antennas, (b) develop a system for sequential firing of the transmitting antennas, (c) perform impedance matching on the antennas for a proper electrical match without the ringing, (d) develop a switching system for transmitting, receiving, and storing of data, and (e) perform image reconstruction of the scatters using imaging algorithms recently developed by the University of Illinois (UI). This system design was to permit many varieties of transmitter pulses of different shapes and frequencies rather than the present design of one fixed type. Newly developed imaging algorithms developed at the UI were to be incorporated into the system for viewing an image of the subsurface defects and objects which exist in the concrete. Also, UI has experience in designing antennas for microwave applications.

UI was to develop the prototype based on the steps listed above. Personnel at the U.S. Army Engineer Waterways Experiment Station (WES) having experience with the NDT of concrete were to consult with the UI about the diagnostic needs of the Corps and help direct the research. Changes were to be recommended and the specifications of the final prototype passed to the manufacturer for manufacturing and marketing.

In this project, the Department of Electrical and Computer Engineering, UI was to develop an ultra-wide-band, (UWB) time-domain impulse and a frequency-domain stepped-frequency radar (SFR) system. At the appropriate stage in the development, the radar system exhibiting the most potential was to be selected for further development. The final system was to be tested at the WES, Vicksburg, MS. WES was to test the performance of the radar unit on various concrete physical models containing rebars, voids, delaminations, etc. A prototype was to be built, tested, modified, manufactured, and marketed.

Scope of Report

This technical report describes the development of the UWB time-domain pulse radar NDE system in detail and illustrates several experimental results. Appendix A presents a bibliography of papers, abstracts, and theses that describe the UWB time-domain NDE system and the SFR frequency-domain system. Appendix B contains a summary of the SFR frequency-domain system from a master's thesis by Mr. Thomas Lee, UI. This report will show that a UWB time-domain impulse radar system was successfully developed.

2 Ultra-Wide-Band Time-Domain Nondestructive Evaluation System

The UWB time-domain microwave impulse radar system is among the new technologies that have the potential for important applications in NDE. The Defense Advanced Research Projects Agency (DARPA) panel defines ultra-wide-band radar as being "any radar whose fractional bandwidth is greater than 0.25, regardless of the center frequency or the signal time-bandwidth product" (DARPA 1990). The fractional bandwidth is defined as $2(f_h - f_l)/(f_h + f_l)$, where f_h is the upper limit of the frequency bandwidth and f_l is the lower limit of the frequency bandwidth.

Compared with conventional narrow-band continuous wave radar systems, the time-domain UWB radar system has several advantages. First, the UWB signal can provide much more information for target sensing purposes. Second, it costs less and takes less measurement time than the coherent SFR system. However, the time-domain system has a lower signal-to-noise ratio (SNR) than the frequency domain system. To improve the SNR in the time-domain system, typical averaging (stacking), time-gating, and wavelets techniques can be applied to suppress the noise level.

The system block diagram of the UWB microwave NDE system is shown in Figure 1. The NDE system consists of a Hewlett-Packard (HP) 54120B digitizing oscilloscope mainframe, an HP 54121A, 20-GHz, four-channel test set, a Picosecond Pulse Lab (PSPL) 4050B voltage step generator, a PSPL 405ORPH remote pulse head, two PSPL 5210 impulse forming networks, two UWB amplifiers, a positioning system with dual stepping motors, and a UWB antenna system. Synchronization of the pulse source and the digitizing oscilloscope is achieved by connecting the PSPL 4050B trigger output port to the HP 54121A test set trigger input port. The pulse repetition rate of the pulsar is 100,000 pulses/sec. There are two different types of UWB antenna systems employed in the UWB microwave NDE system: the Vivaldi antenna (Frantz 1992) array and the ridge horn synthetic aperture radar (SAR) system. The whole NDE system is controlled and automated by a personal computer via the Institute of Electrical and Electronic Engineers 488 bus. The PSPL 4050B step generator

with the PSPL 405ORPH remote pulse head generates a 10-volt, 45-ps rise-time pulse. A 1.5-volt, 10-GHz monocycle pulse is generated by attaching two PSPL 5210 impulse forming networks. The monocycle pulse is used as the transmitting source in order to match the operational frequency bandwidth of the antennas. The time-domain plot and the frequency spectrum of the monocycle pulse are shown in Figure 2. The transmitting monocycle pulse source signal does satisfy the UWB definition. Figure 3 shows the Vivaldi antenna and Vivaldi antenna array. The Vivaldi antenna array consists of five transmitting antennas and six receiving antennas. Those antennas are separated by 80 mm each. Figure 4 shows the ridge horn antenna SAR system.

The SAR system consists of a pair of ridge horn antennas, a positioning system using dual stepping motors, and a two-dimensional positioning table. The UWB amplifier at the transmitting port is a 30-db gain, 23-dbm output power amplifier (Miteq MPN4-01001800-23P), and the low noise amplifier at the receiving port is a 20-db gain, 10-dbm output power amplifier (Miteq AFS3-001010000-38-LN). The UWB time-domain NDE system offers a less expensive alternative to the other coherent SFR system developed at the University of Illinois, Champaign, IL, based on the HP8510B network analyzer.

Figures 5 and 6 show the typical time-domain measurement data of a metallic cylinder and a plastic pipe, respectively. Figure 5(a) is the measured data of the clutter of the system without a test target. The clutter includes background and coupling noise between the transmitting antenna and receiving antenna. Figure 5(b) shows the measured data of the metallic cylinder. Figure 5(c) shows the subtraction of the clutter from the measured metallic cylinder data. The single reflected pulse from the metallic cylinder can be clearly seen. Figure 6(a) is the measured data of the clutter of the system without a test target. Figure 6(b) shows the measured data of the plastic pipe. Figure 6 (c) shows the subtraction of the clutter from the measured plastic pipe data. The multiple reflected pulses from the plastic pipe can be clearly seen.

Before adopting the two Miteq amplifiers, investigators also tried to add the HP83006A amplifier to the UWB time-domain NDE system to increase the transmitting power. The collected measurement data are shown in Figures 7 and 8. Figure 7(a) is the measured data of the clutter of the system without a test target. The clutter includes background noise and a coupling between the transmitting antenna and receiving antenna. Figure 7(b) shows the measured data of the metallic cylinder. In Figure 7(c), clutter is subtracted from the measured metallic cylinder data. The single reflected pulse from the metallic cylinder can be clearly seen.

Figure 8(a) is the measured data of the clutter of the system without the test target. Figure 8(b) shows the measured data of the plastic pipe. In Figure 8(c), clutter is subtracted from the measured plastic pipe data. Multiple reflected pulses from the plastic pipe can be clearly observed.

From Figures 7 and 8 results, researchers understood that the prototype time-domain pulse radar system was working. However, the output power was still

not high enough. The above measurement utilized the largest number of averages available in the HP54121T digitizing sampling oscilloscope (2,048), in order to increase the SNR. However, it took about 20 min to do one set of measurements. Using the Vivaldi antenna array, it would take approximately 10 hr for the 30 sets of measurements. Therefore, it was not practical to take these measurements and the two Miteq amplifiers were used at the transmitting and receiving ports in order to increase the dynamic range of the system.

The patterns of the Vivaldi antenna at different frequencies are shown in Figures 9-13. Figure 9 shows the pattern at 1 Ghz, Figure 10 shows the pattern at 2 Ghz and Figure 11 shows the pattern at 3 GHz. From these three figures, it can be seen that the antenna has higher directivity at higher frequencies because the beam width decreases when the frequency increases. Figure 12 shows the co-polarization and cross-polarization patterns at 2 GHz. Figure 13 shows the co-polarization and cross-polarization patterns at 3 GHz. From these two figures, it can be seen that the co-polarization and cross-polarization have good polarization isolation and are higher than 20 db. The gain of the Vivaldi antenna is shown in Figure 14. The higher gain at the higher frequencies is consistent with higher directivity at the higher frequencies shown in Figures 9-11.

3 Data Acquisition and Calibration

The impulse radar system has been evaluated by collecting useful measurement data (30 sets) from the 5 transmitting and 6 receiving antennas using the Vivaldi antenna array. Figure 15 shows cluttered measurement data sets for the system without the test target. Clutter includes background and coupling noise between the transmitting antenna and receiving antenna.

In Figure 15, a strong coupling effect was noticed between the transmitting antennas and receiving antennas of the Vivaldi antenna array around the time axis at 1 ns. Figure 16 shows metallic cylinder (M) measurement data. In Figure 16, a small target signal embedded in the time axis within a 3-ns to 4-ns range can be identified. In Figure 17, the clutter data are subtracted from the metallic cylinder measurement data. From Figure 17, the single reflected pulse signal from the metallic cylinder can be clearly seen. However, this received reflected signal is not the actual value of the scattered field of the metallic cylinder; it is the value of the actual scattered field convolved with the system response (S) of the impulse radar system. Therefore, the effect of the system response must be removed by a deconvolution process in order to obtain the actual scattered field value. This can be achieved by measuring a known reference target at a known position. The actual scattered field (T) of this reference target is known. The system response is equal to (R-C) deconvolved with T, where R is the measured reference target scattered field data, C is the measured clutter data, and T is the actual scattered field of the reference target.

After the system response value is obtained, the actual scattered field value of the metallic cylinder can be obtained by an additional deconvolution process to remove the system response of the impulse radar system. The actual scattered field value of the metallic cylinder is equal to (M-C) deconvolved with S, where M is the measured metallic cylinder scattered field, C is the measured clutter data, and S is the system response effect. The calibrated result is shown in Figure 18. Figure 19 shows the one-dimensional SAR time-domain measurement data using a pair of ridge horn antennas. The test target is an embedded metallic cylinder (25-mm radius) located 150 mm beneath a concrete slab surface. Figure 20 shows the data from Figure 19 after background subtraction. The reflected signal of the embedded target can be clearly observed.

In order to improve the SNR of the time-domain system, the time-gating function, the averaging (stacking), and wavelet techniques (Donoho 1993, 1995) can be applied to the time-domain measurement data. The time-gating function can be applied to the measurement data in order to remove the unwanted early-time and late-time arrival signal. Statistical errors can be reduced by an internal averaging function of the digital sampling oscilloscope. The averaging number is up to 2,048 in the HP 54120B digitizing oscilloscope mainframe. For example, the noise level is reduced by the factor of $\sqrt{n}$, that is, 8-db reduction for $n = 64$. The wavelet technique can also be applied to denoise the time-domain measurement data (Donoho 1993, 1995). Figure 21 shows the noise reduction when the wavelet technique is applied to the measured time-domain signal.

4 Inverse Scattering Imaging

The inverse scattering problem is quite difficult to solve because the high spatial frequency portions of the test target, which causes the evanescent waves, cannot be measured. Besides, the multiple scattering phenomenon causes the inverse scattering problem to be a nonlinear problem. As well as being nonlinear and non-unique, the inverse scattering problem is often ill-posed due to limited measurement data available caused by the geometry problem and the measurement system limitation.

The 30 calibrated measurement data sets can be processed by inverse scattering imaging algorithms to obtain the reconstructed image of the test target. Two nonlinear iterative inverse scattering imaging algorithms, the Distorted Born Iterative Method (DBIM) (Chew 1990, Chew and Wang 1990) and the Local Shape Function (LSF) method (Chew and Otto 1992, Otto and Chew 1994) have been applied successfully to process the measurement data.

However, when the multiple scattering phenomenon is not important, the first-order Born approximation method such as diffraction tomography can be used in order to reduce the intensive computational time of DBIM and LSF.

Figure 22 shows the reconstructed image of a metallic cylinder using the LSF method. The front curvature of the cylinder facing the Vivaldi antenna array is clearly observed. Figure 23 shows the reconstructed image of two metallic cylindrical rods using the LSF method. Figure 24 shows the reconstructed image of a polyvinyl chloride (PVC) pipe using DBIM permittivity reconstruction. The circular shape of the PVC pipe can be clearly observed, and the reconstructed permittivity value of the PVC pipe is close to the actual value of 2.5. Figure 25 shows the reconstructed image of a small metallic cylinder embedded in a concrete block using the LSF algorithm. The upper curvature is the shape of the concrete block. The lower part of the image is the small metallic cylinder embedded 20 mm beneath the concrete block surface. Figure 26 shows the diffraction tomography (Devaney 1982) reconstruction image of a metallic cylinder (50-mm diameter) embedded 150 mm beneath a cement slab.

5 Field Test and Results

Field Test

The time-domain pulse radar NDE system has been demonstrated successfully in a field test WES in Vicksburg, MS. The time-domain impulse radar system has demonstrated the capability of detecting small reinforcing bars embedded in large concrete blocks in the field test demonstration.

Figures 27-29 show data collected from the field test at WES. Figure 27 shows data collected for test sample I, a small reinforcing bar (11.1-mm radius) embedded in a concrete slab. The hyperbolic curve of the reinforcing bar can be clearly observed from the time-domain measurement data trace. Figure 28 shows data collected for test sample II, reinforcing bars (9.5-mm radius) embedded in a concrete slab. Six hyperbolic curves can be clearly observed. Figure 29 shows data collected from test sample III, five smaller reinforcing bars (6.35-mm radius) embedded in a concrete slab. Those data have been processed by inverse scattering algorithms described above. The reconstruction images of these data will be analyzed at a later time.

Results

A number of major attributes of a radar unit were developed in the investigation: fabrication and evaluation of two types of antennas to get proper directivity and improve polarization isolation, evaluation of a number of image reconstruction algorithms, evaluation of two different types of radar (time-domain and frequency-domain systems), development of equipment to develop a synthetic aperture radar, development of a UWB system, improvement of the rate of data collection, and improvement of the SNR with various techniques, computer control of the system, etc.

6 Conclusions, Recommendations, and Commercialization

Conclusions

A UWB time-domain microwave imaging radar system has been successfully developed for detecting shallow buried objects in concrete. This system successfully combined the time-domain impulse radar system hardware and inverse scattering imaging software. The imaging radar system shows a high potential for use in the nondestructive evaluation and quality control of civil structures. This microwave UWB time-domain NDE system has several features that do not exist in commercial systems on the market: low power and ultra-wide bandwidth. The system can achieve a high-resolution image with test targets located in air or in shallow subsurfaces. Its UWB frequency bandwidth can provide much more information for target sensing, classification, and evaluation purposes.

The development of the new radar unit was not brought to its final stage of completion due to the many individual features of the radar unit that required development: multiple antennas, electrical matching, increased power level, imaging, resolution, etc. The scope of the investigation turned out to be larger than could be accomplished within the given time and within the allocated funds. Although obstacles were expected in the research, it was not evident in the beginning of the project that much time would be consumed in developing a few of the features. In hindsight, advancing the state of the art of radar by improving just one or two features of an existing type of GPR unit would have been a more reasonable objective than trying to develop a whole new model.

One of the primary deficiencies of the new system is that the power of transmission was short of the goal for penetration into thick concrete structures. The radar performs well for depths of 150 mm or less, but the output power needs to be increased to get penetration depths of a few meters.

Although the research project consisted of a sound and objective scientific investigation and the state of radar was advanced, the goal of achieving an

improved radar system for field purposes was not accomplished. Although one cannot always guarantee the outcome of a project, it was felt that the state of radar for concrete was advanced and a descriptive report of the results (positive as well as negative results) should be provided on the project investigation.

Recommendations

Advancements made in developing the new radar unit should continue to be promoted through technology transfer and funds sought to improve the development of the system by employing (a) laboratory physical concrete models with known mechanical properties and well-defined artificial defects, and (b) field structures, both of known and unknown condition. Definite plans should be laid out in a proposal by UI for increasing the penetration distance and making the system suitable for commercialization. Field tests should be proposed to validate the capability of the new system.

The U.S. Army Corps of Engineers still needs an improved radar system for concrete. An ultimate goal for any diagnostic system is to provide an image of the evaluation object rather than some echo signature or some graphic that combines many echo signatures, and this project has had some success in that area.

Commercialization

The system is not ready for commercialization, at least, for Corps of Engineer structures.

References

Chew, W. C. (1990). *Waves and fields in inhomogeneous media.* Van Nostrand, New York.

Chew, W. C., and Otto, G. P. (1992). "Microwave imaging of multiple metallic cylinders using shape functions," *Micro. Guided Wave Lett* 2(7), 284-286.

Chew, W. C., and Wang, Y. M. (1990). "Reconstruction of two-dimensional permittivity distribution using the distorted born iterative method." *IEEE Trans. Medical Imag.* (9)2, 218-225.

Defense Advanced Research Projects Agency. (1990). "Ultra-wideband radar review panel," *Assessment of Ultra-Wideband (UWB) Technology,* Arlington, VA.

Devaney, A. J. (1982). "A filtered back-propagation algorithm for diffraction tomography," *Ultrasonic Imaging* (4), 336-360.

Donoho, D. L. (1993). "Progress in wavelet analysis and WVD: A ten minute tour," *Progress in Wavelet Analysis and Application*, 109-128.

_____. (1995). "De-noising by soft-thresholding." *IEEE Trans. on Inf. Theory* 41(3), 613-627.

Frantz, K. M. (1992). "An investigation of the vivaldi flared radiator," M. S. thesis, University of Illinois at Urbana-Champaign.

Otto, G. P., and Chew, W. C. (1994). "Microwave inverse scattering — local shape function (LSF) imaging for improved resolution of strong scatters." *IEEE Trans. Microwave Theory Tech. (MTT-42)* 1, 137-141.

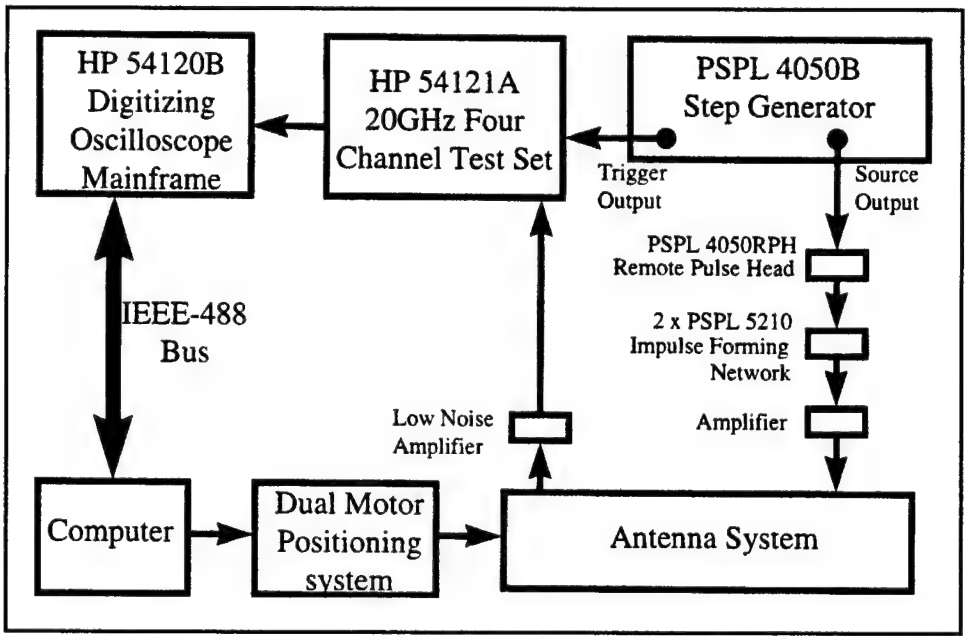

Figure 1. The UWB time-domain microwave NDE system

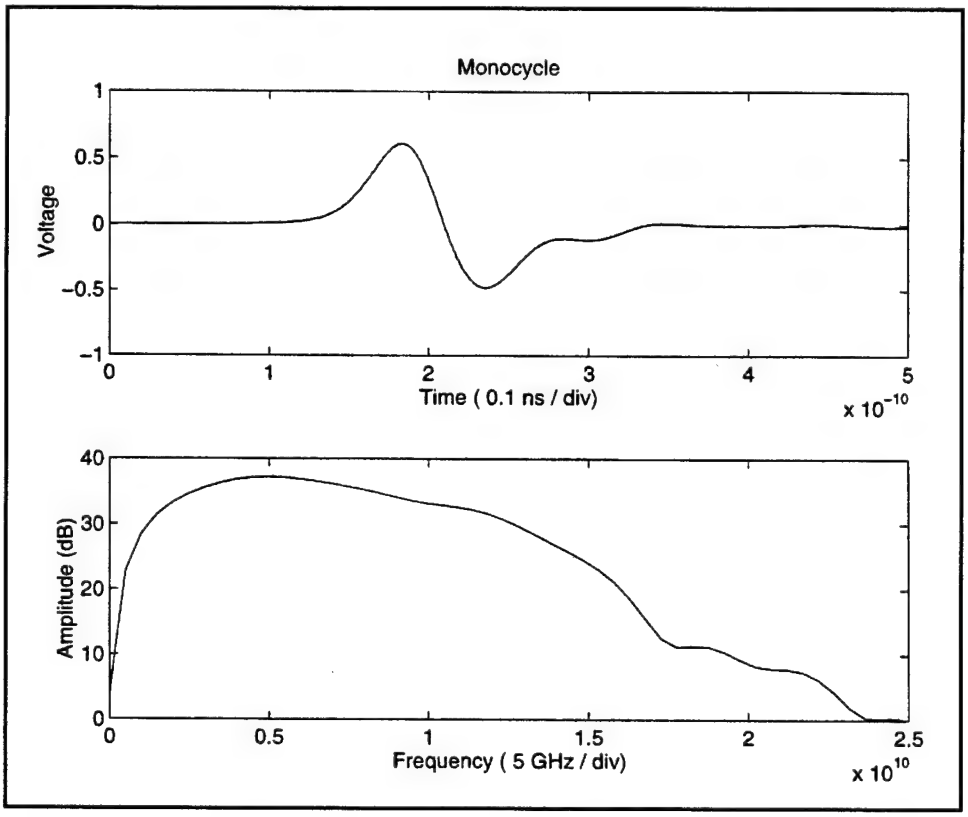

Figure 2. The time-domain profile and frequency spectrum of the monocycle pulse source

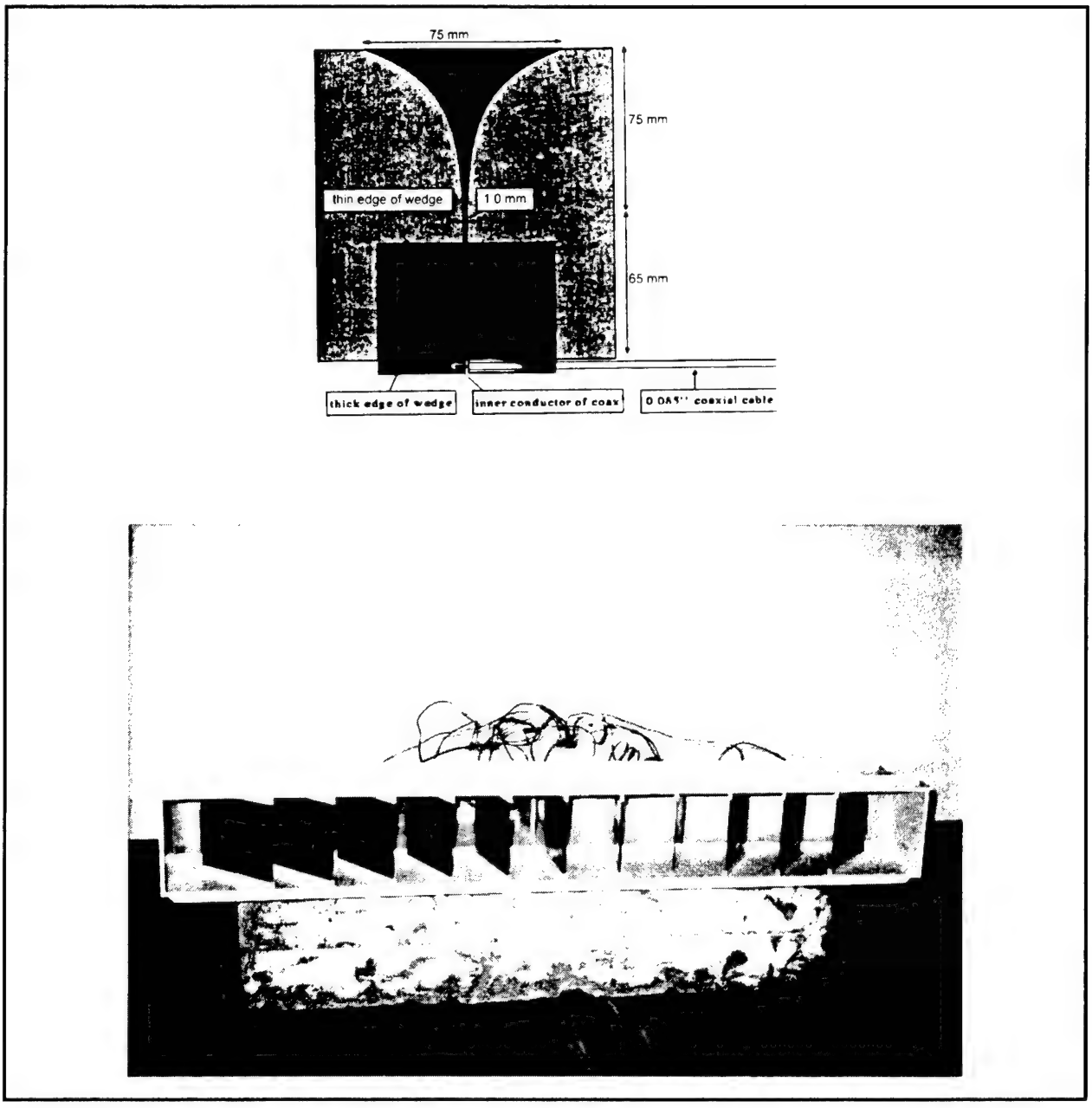

Figure 3. The Vivaldi antenna and Vivaldi antenna array

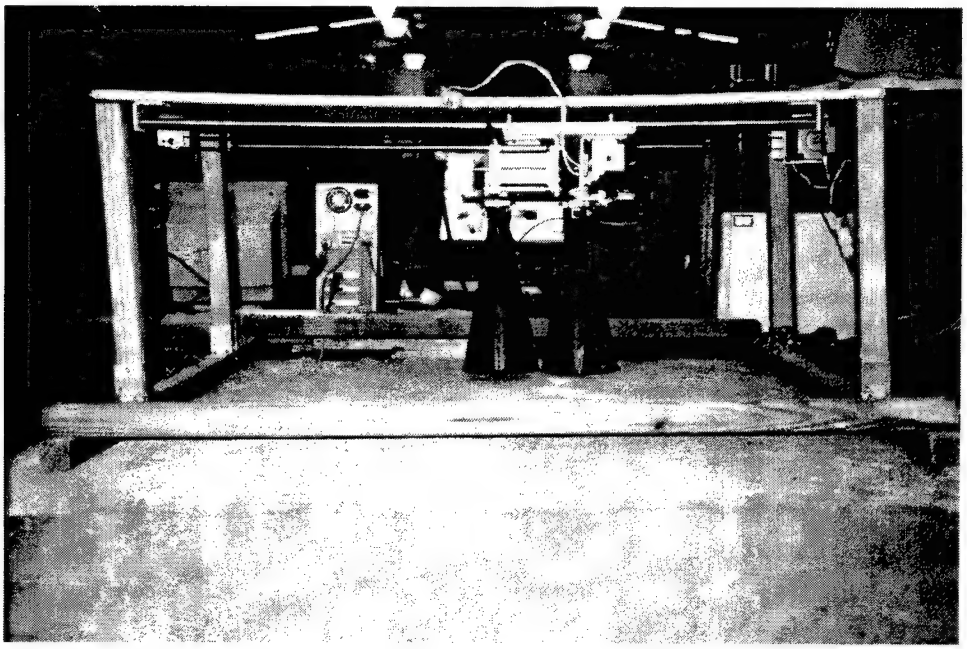

Figure 4. The ridge horn antennas of the SAR system

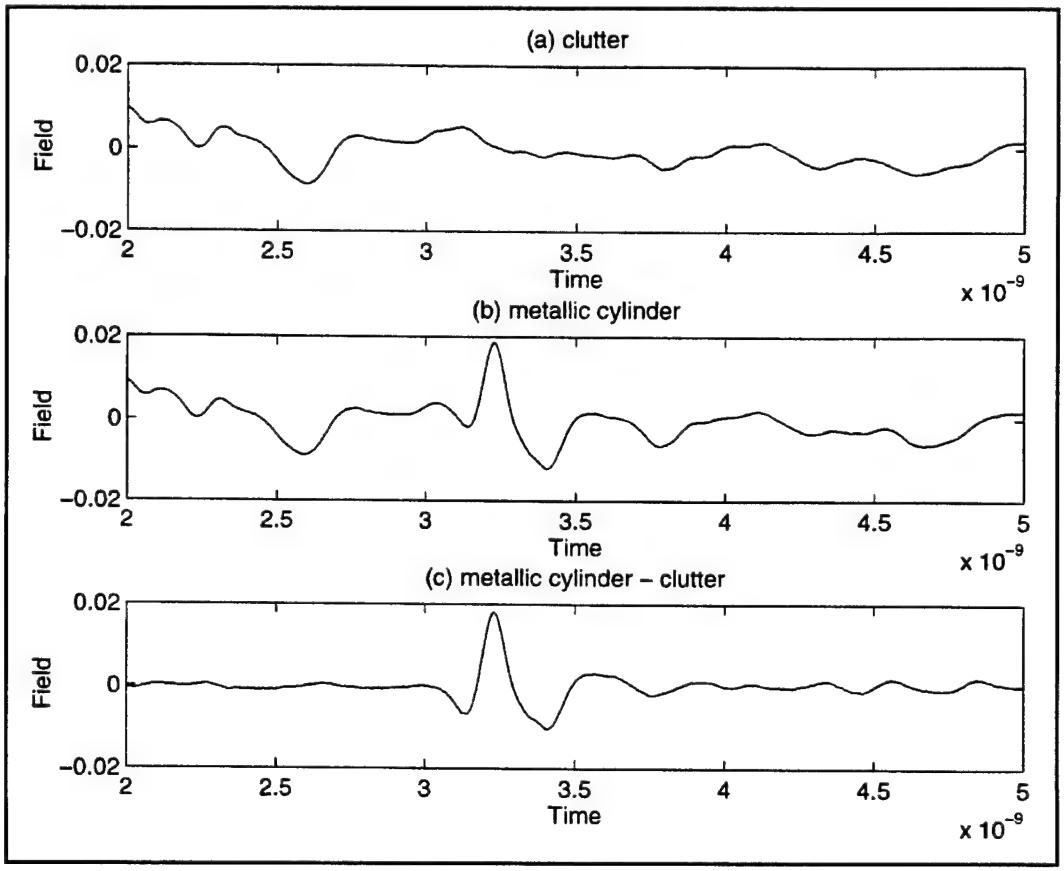

Figure 5. The time-domain measurement data of metallic cylinder

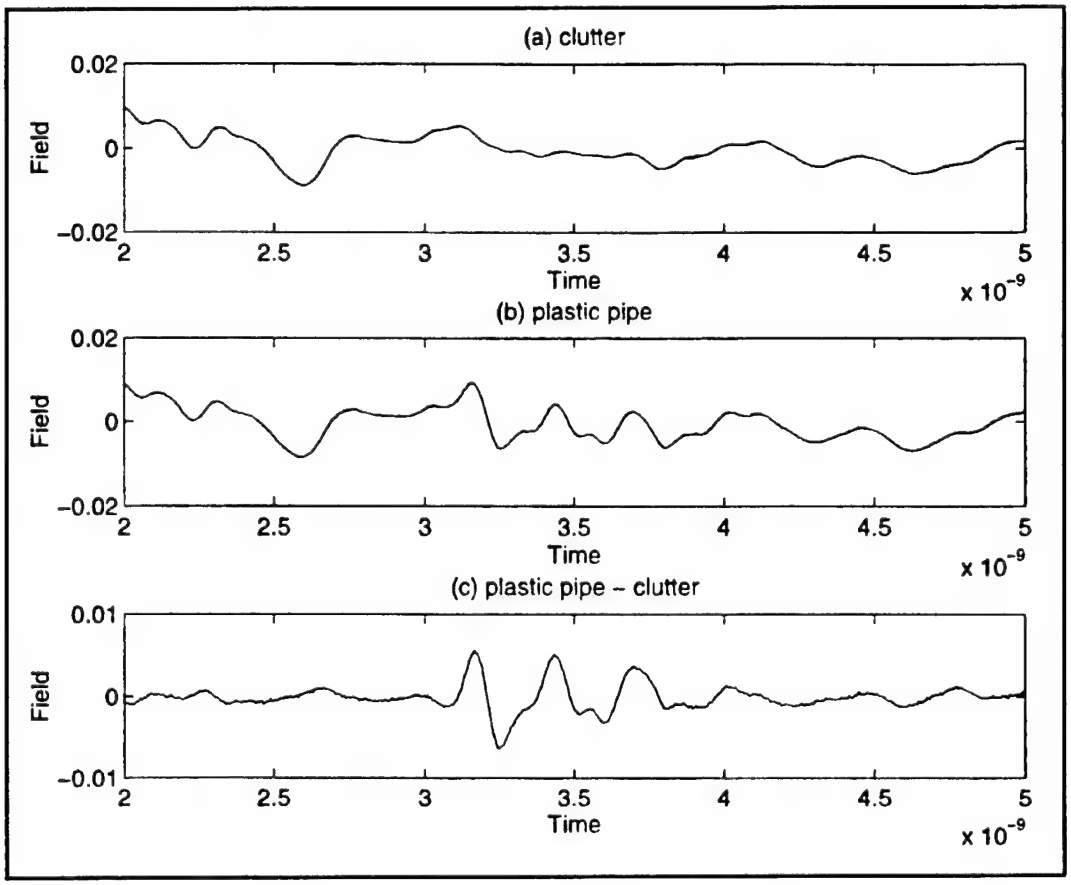

Figure 6. The time-domain measurement data of plastic pipe

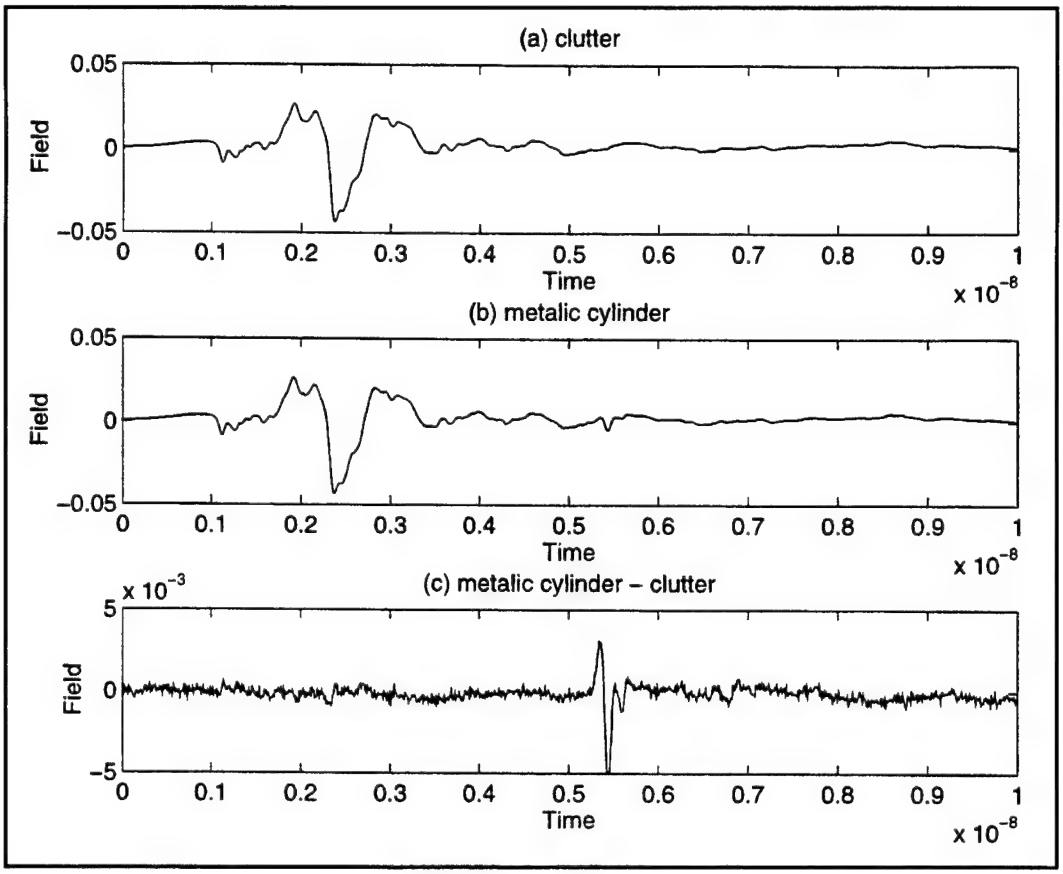

Figure 7. The time-domain measurement data of metallic cylinder

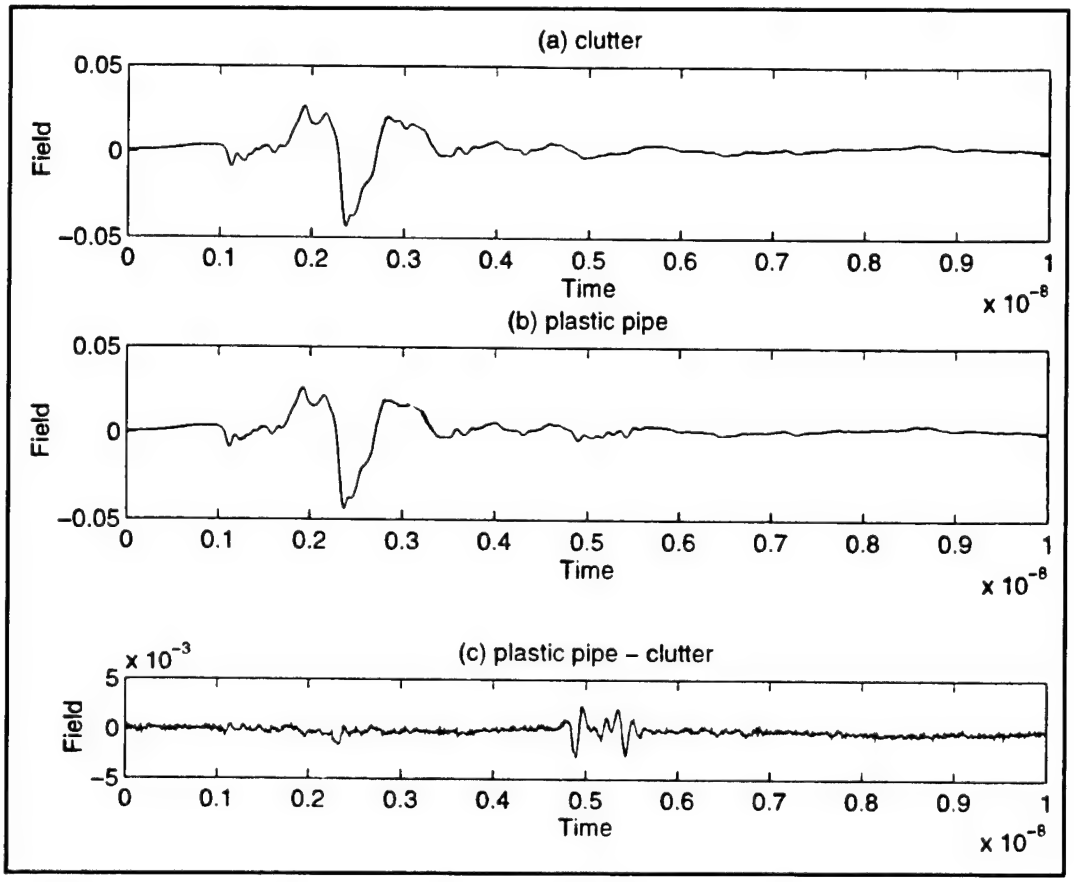

Figure 8. The time-domain measurement data of plastic pipe

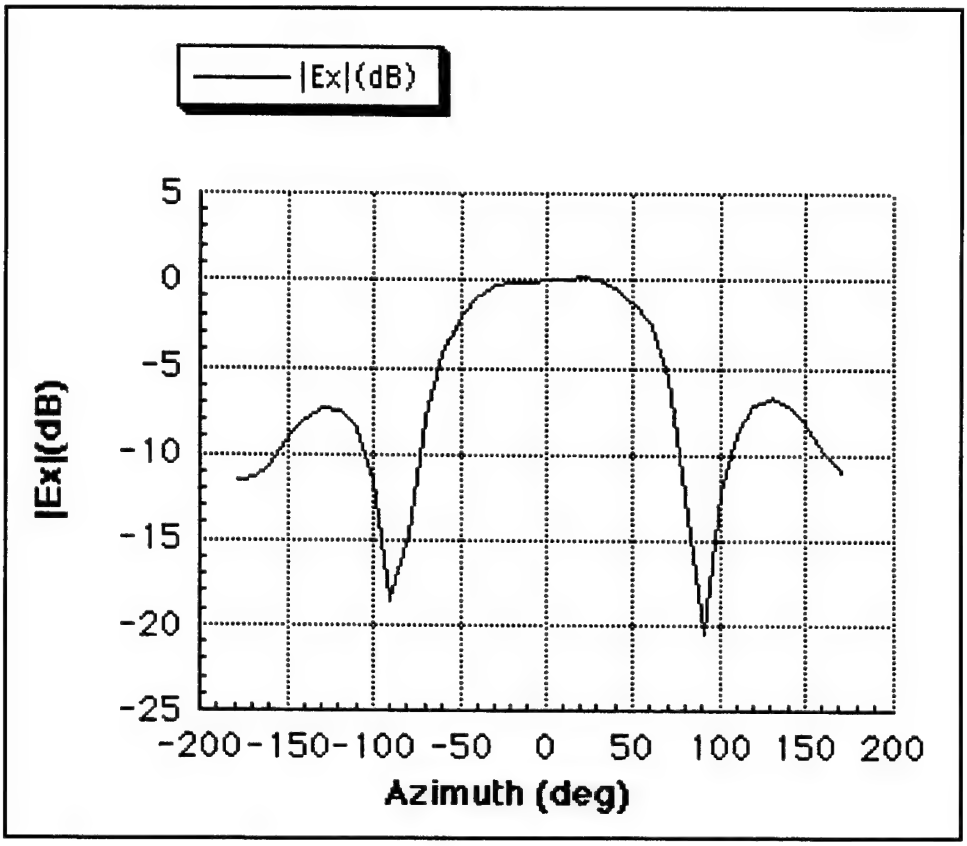

Figure 9. The antenna pattern of the Vivaldi antenna at 1 GHz

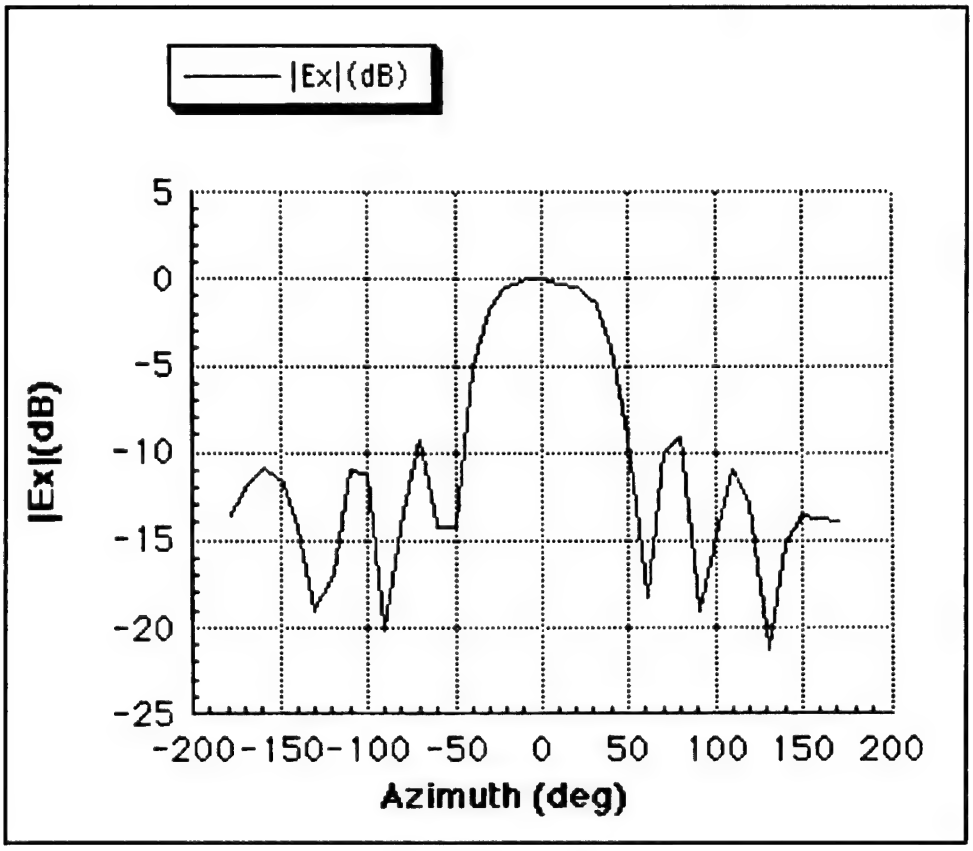

Figure 10. The antenna pattern of the Vivaldi antenna at 2 GHz

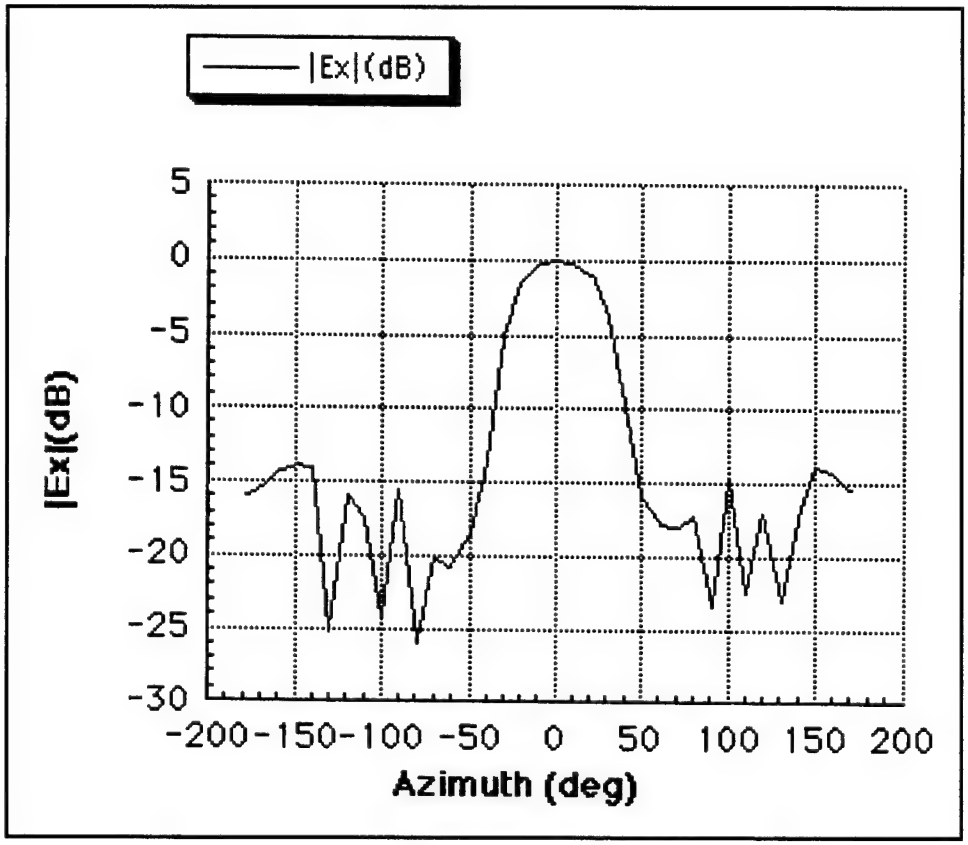

Figure 11. The antenna pattern of the Vivaldi antenna at 3 GHz

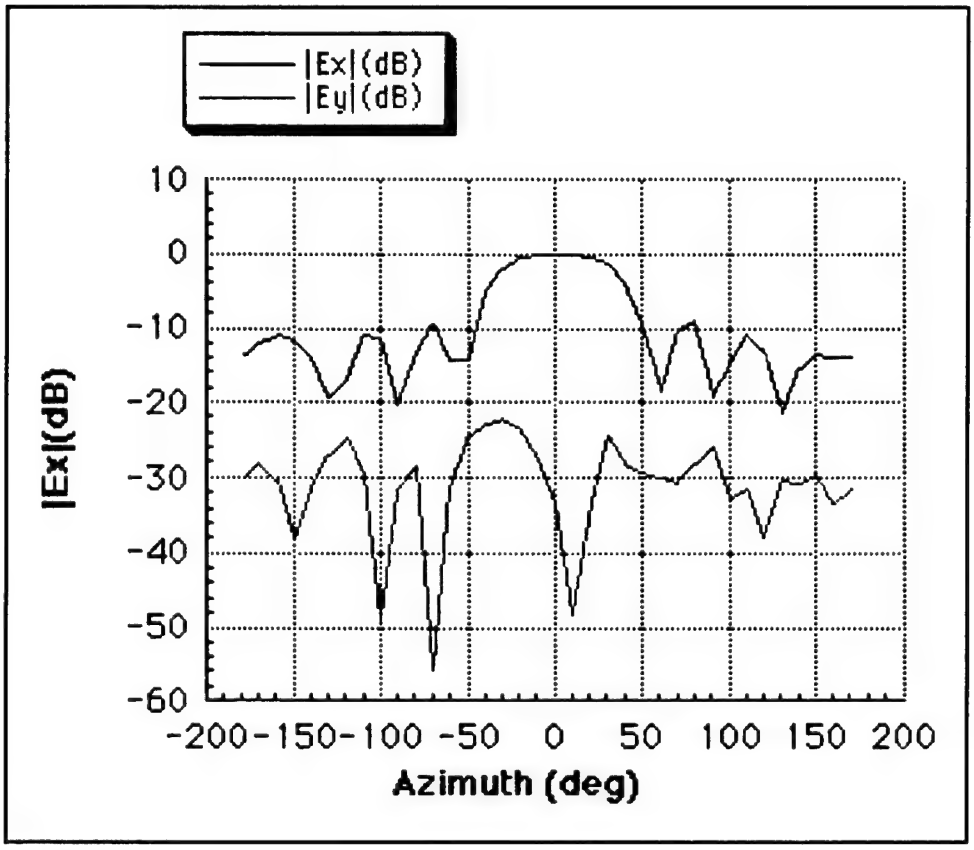

Figure 12. The co-pol (Ex) and cross-pol (Ey) antenna pattern of the Vivaldi antenna at 2 GHz

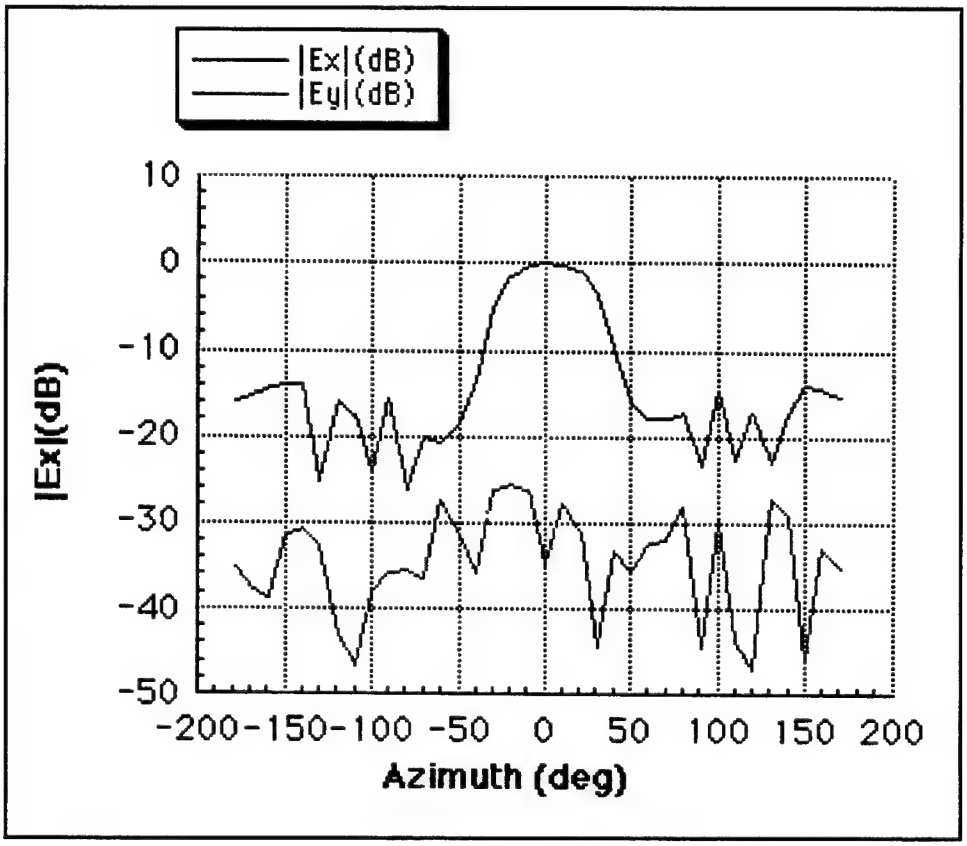

Figure 13. The co-pol (Ex) and cross-pol (Ey) antenna pattern of the Vivaldi antenna at 3 GHz

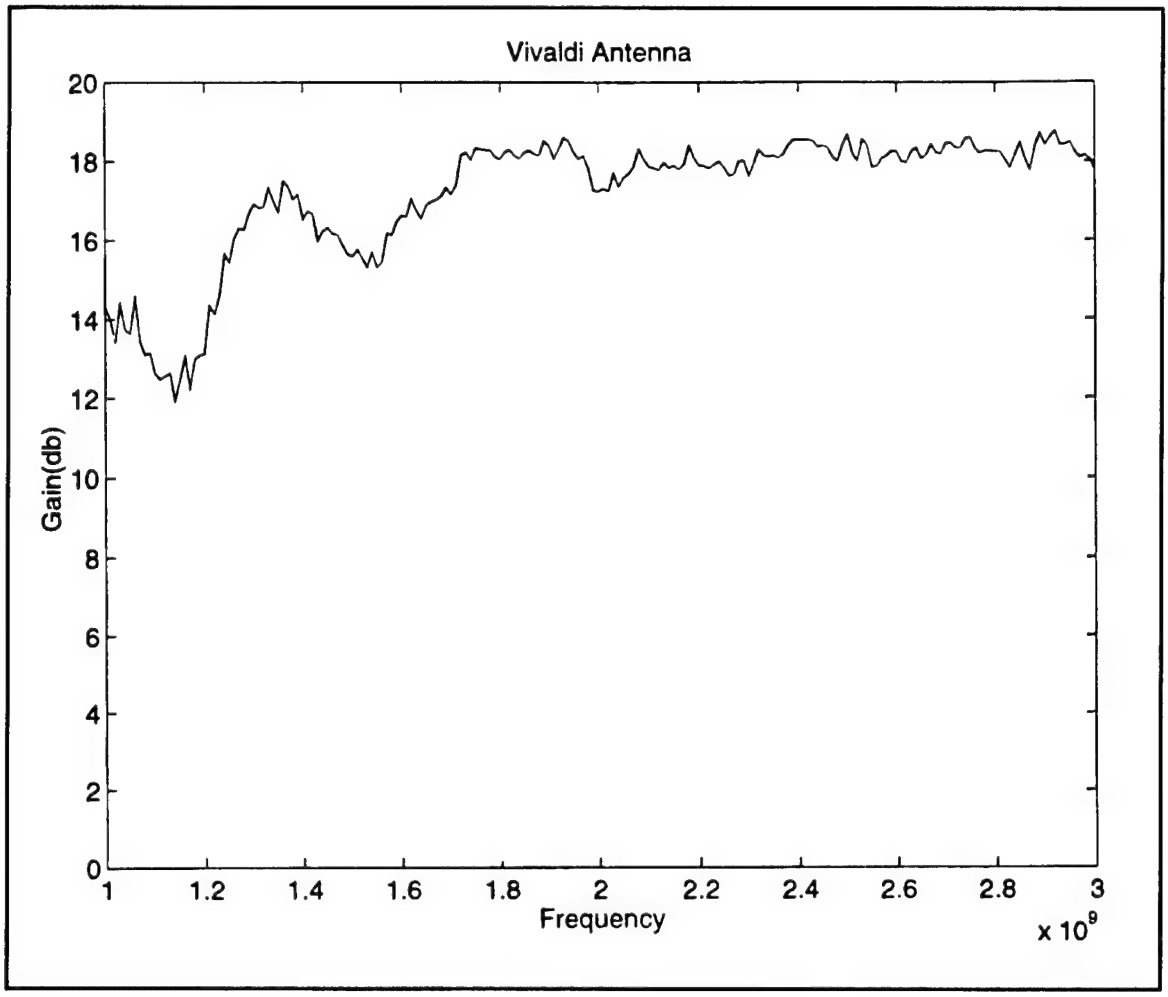

Figure 14. The antenna gain of the Vivaldi antenna

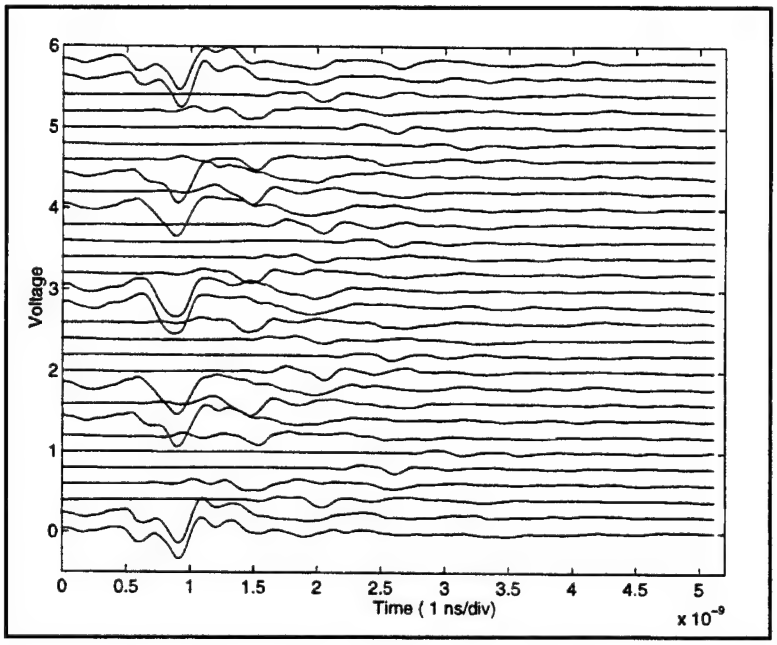

Figure 15. Clutter measurement data (30 sets from the 5 transmitting antennas and 6 receiving antennas)

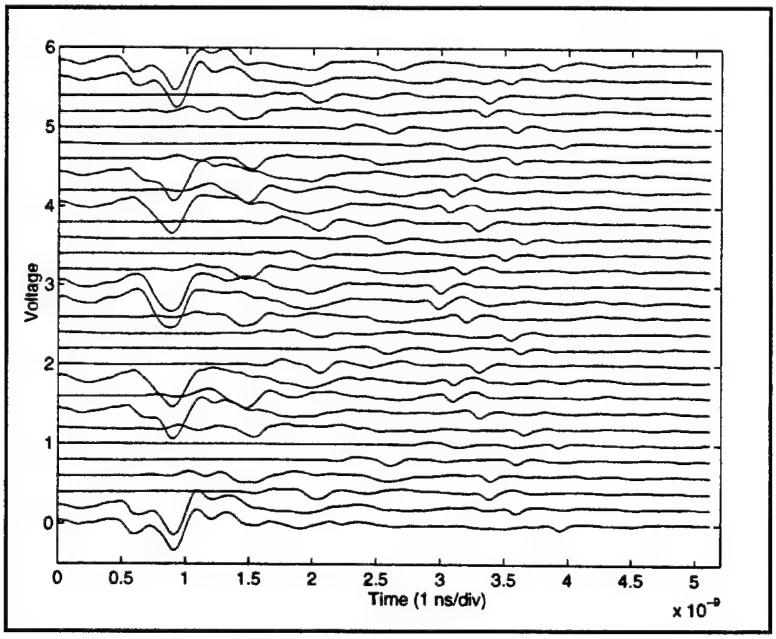

Figure 16. Metallic cylinder (3.2 cm in diameter measurement data (30 sets from the 5 transmitting antennas and 6 receiving antennas)

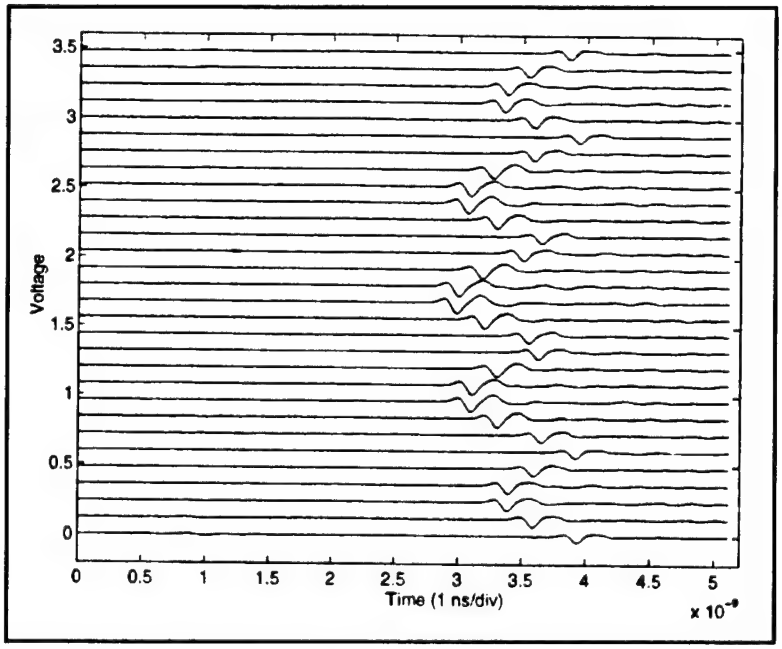

Figure 17. Subtraction of the clutter measurement data (Figure 15) from the metallic cylinder measurement data (Figure 16)

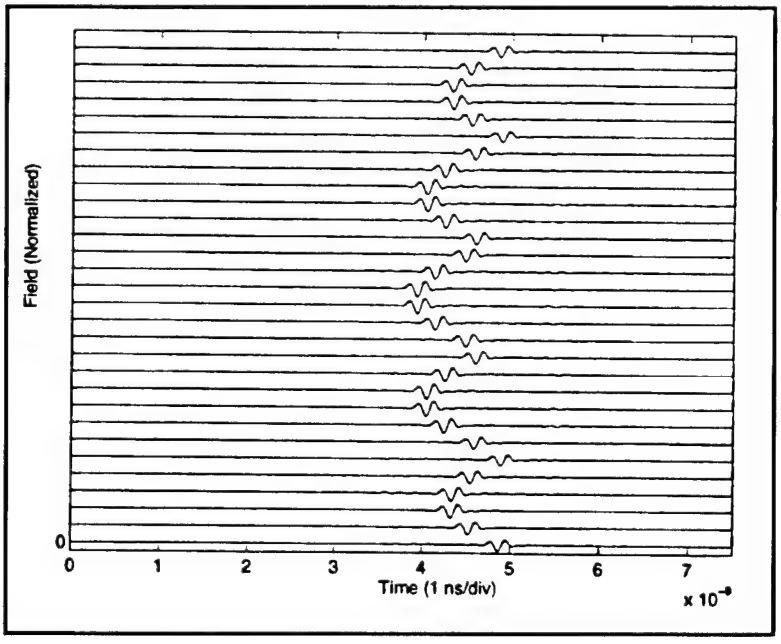

Figure 18. Calibrated normalized electrical field of the metallic cylinder

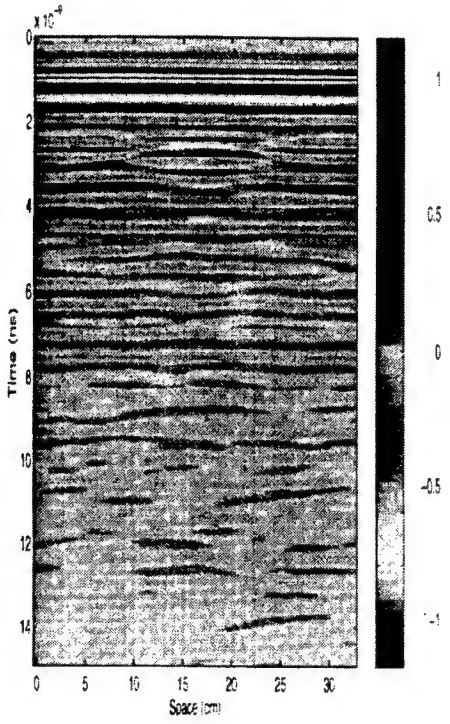

Figure 19. Raw time-domain measurement data of a metallic cylinder embedded in a concrete slab

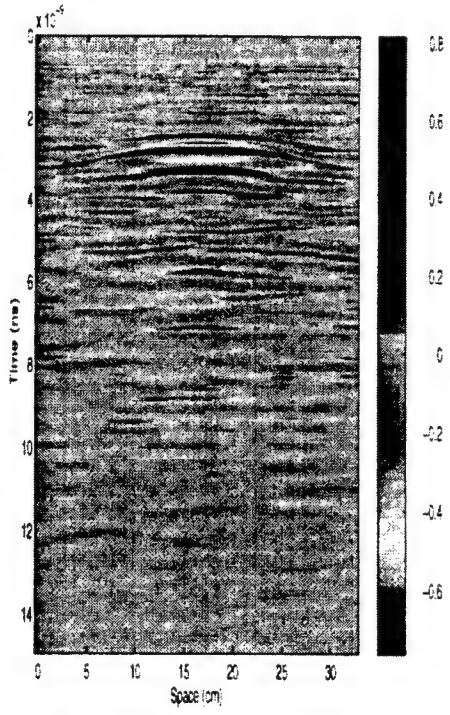

Figure 20. Time-domain measurement data of Figure 19 after background subtraction

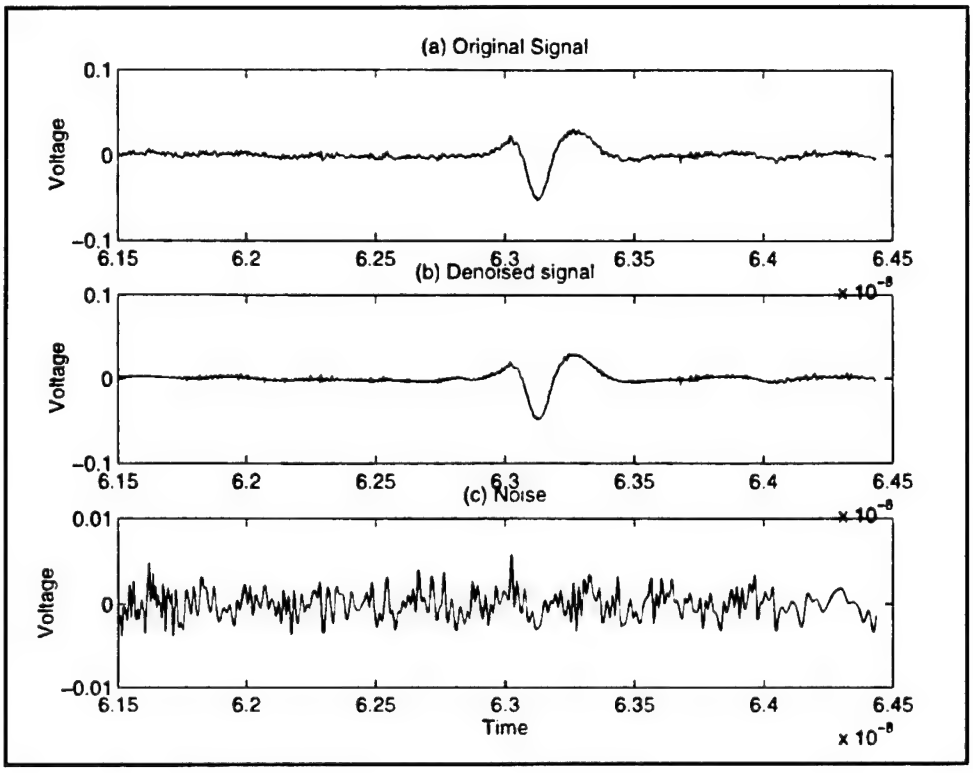

Figure 21. Applying the wavelet technique to denoise the time-domain measurement data

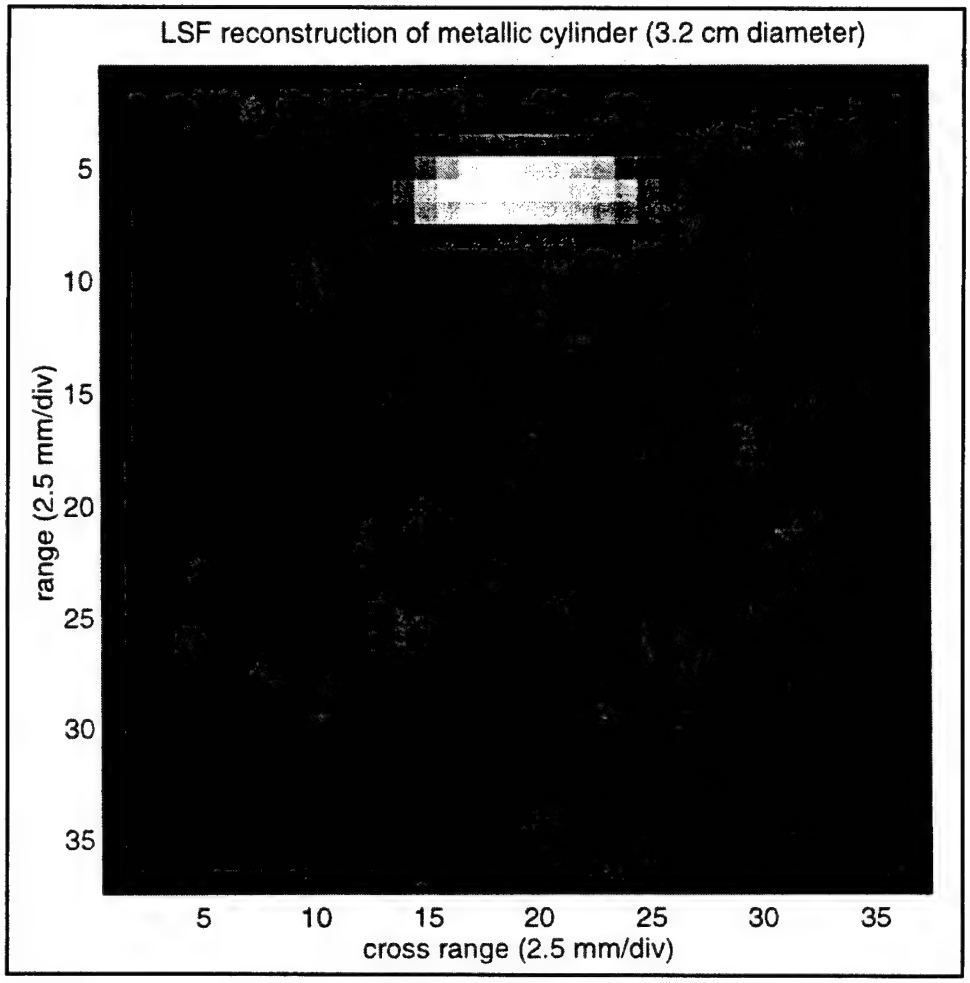

Figure 22. Reconstructed image of the metallic cylinder

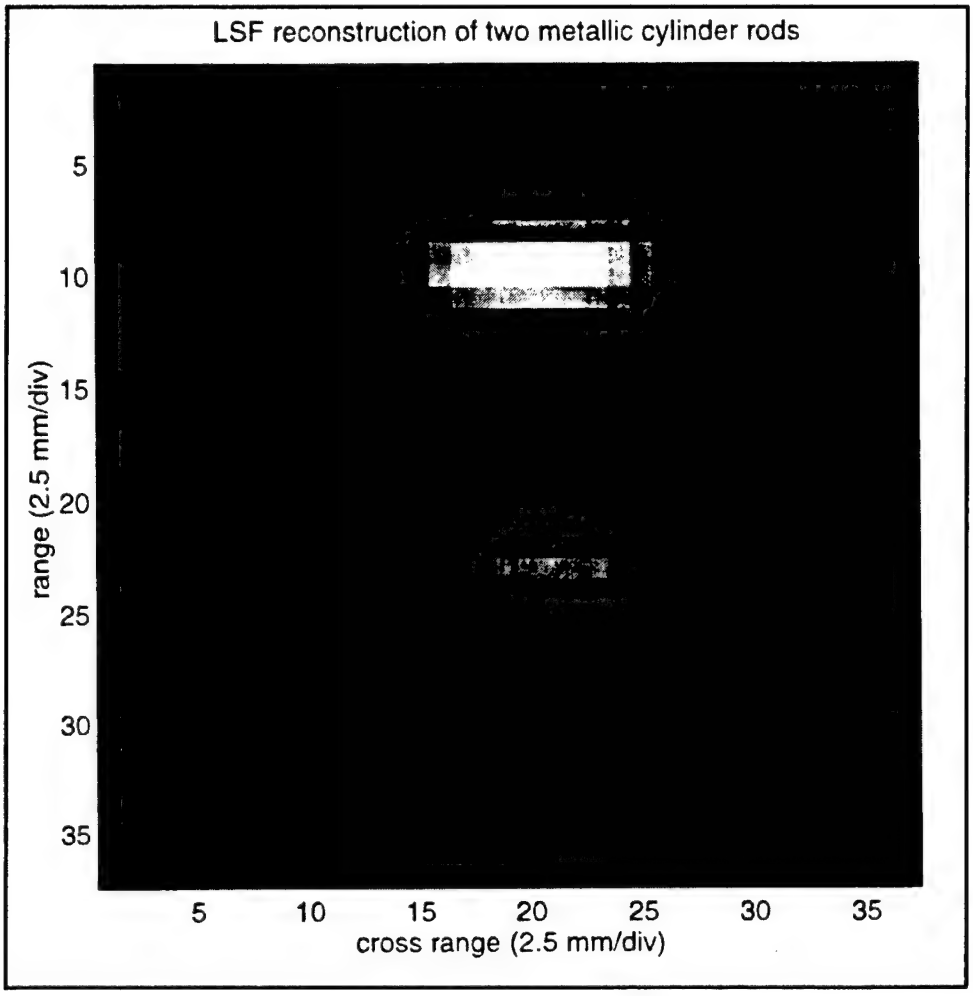

Figure 23. Reconstructed image of two metallic cylinder rods

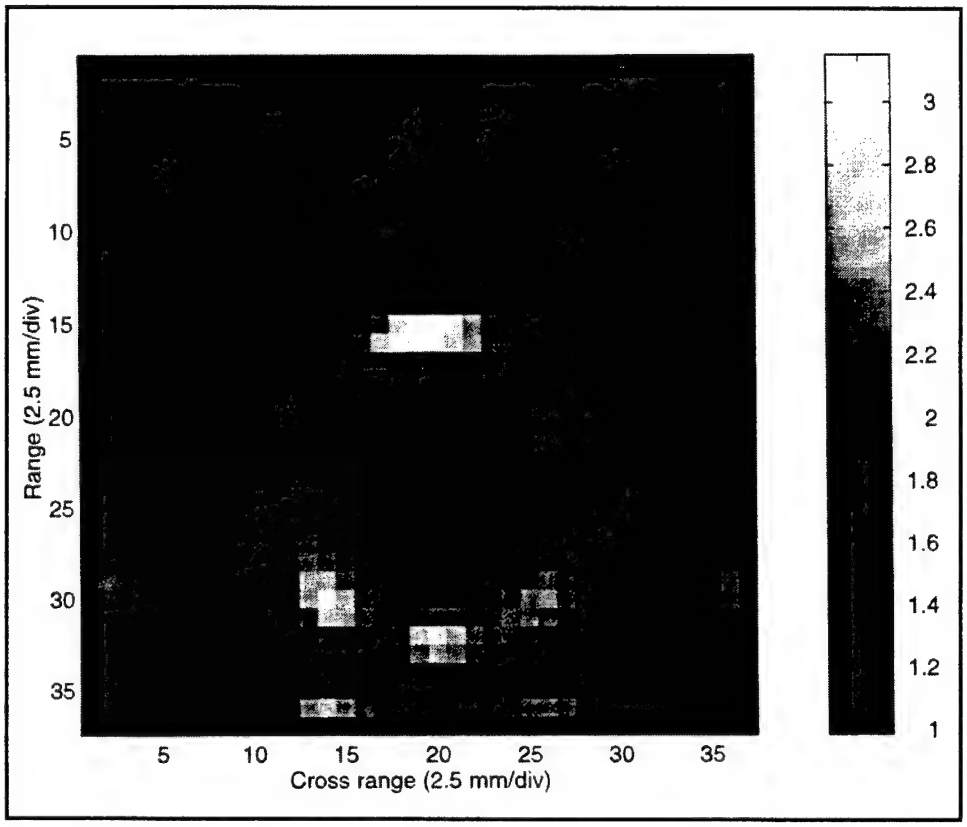

Figure 24. DBIM reconstructed image of a plastic PVC pipe (4.8 cm in diameter)

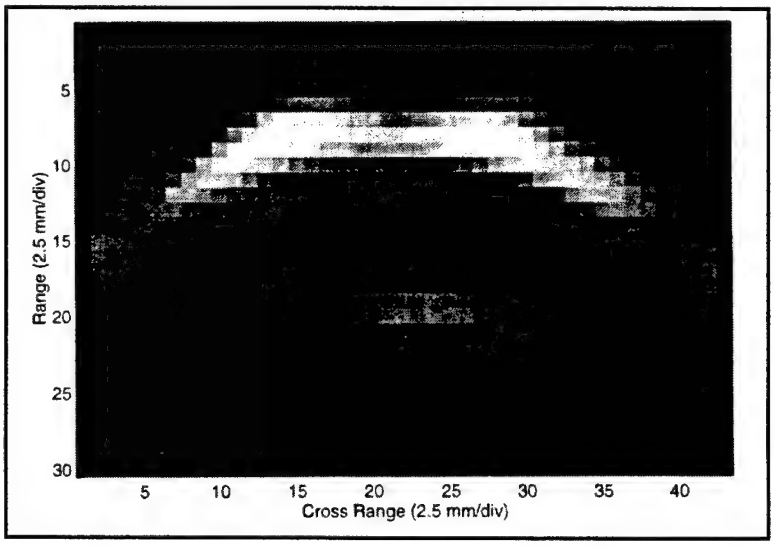

Figure 25. LSF reconstructed image of a small metallic cylinder (1 cm in diameter) embedded 2 cm beneath a concrete cement block

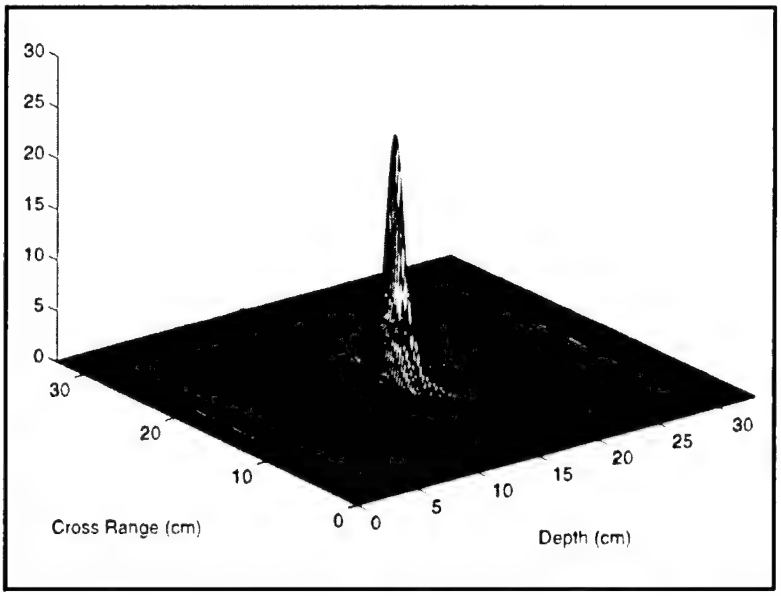

Figure 26. Diffraction tomography reconstruction image of a metallic cylinder embedded in a cement slab

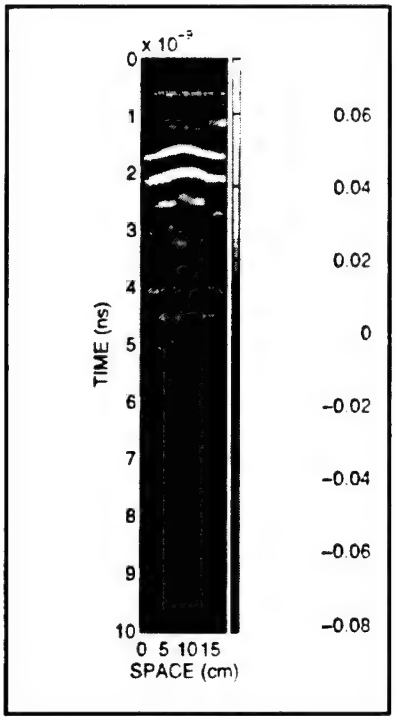

Figure 27. Collected data of test sample I from WES

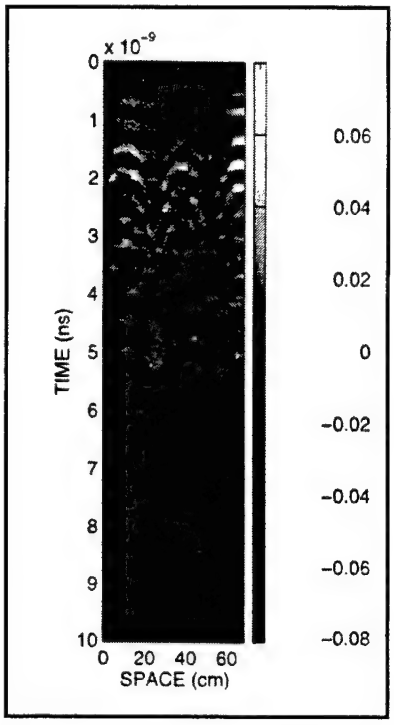

Figure 28. Collected data of test sample II from WES

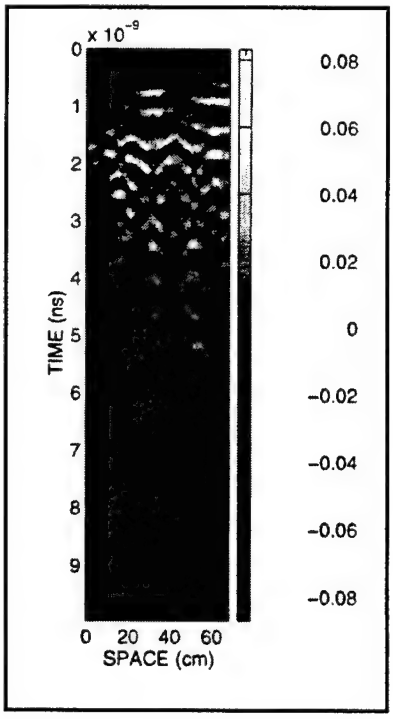

Figure 29. Collected data of test sample III from WES

Appendix A
Technology Transfer of Ultra-Wide-Band Time-Domain Nondestructive Evaluation System

To promote the ultra-wide-band (UWB) time-domain nondestructive evaluation (NDE) system, researchers at the University of Illinois have presented the UWB time-domain NDE system in seven conferences (four papers and three abstracts) as follows.

Papers

Chen, F. -C., and Chew, W. C. (August 1997). "Microwave imaging radar system for detecting buried objects," *IGARSS'97,* Singapore.

_____. (July 1997). "Development and testing of the time-domain microwave nondestructive evaluation system," *Twenty-fourth Annual Review of Progress in Quantitative Nondestructive Evaluation,* San Diego, CA.

_____. (1996a). "Ultra-wideband imaging radar system," *URSI Radio Science Meeting Digest,* Montreal, Canada.

_____. (1996b). "Time-domain ultra-wideband radar system for nondestructive evaluation," *URSI Radio Science Meeting Digest,* Baltimore, MD.

Abstracts

Chen, F.-C., and Chew, W. C. (1996a). "An impulse radar nondestructive evaluation system," *Twenty-third Annual Review of Progress in Quantitative Nondestructive Evaluation*, Brunswick, ME.

_____. (1996b). "Time-domain pulse system for inverse scattering and imaging," *Antenna Applications Symposium,* Monticello, IL.

Chen, F.-C., Chew, W. C., and Weedon, W. H. (July 1996). "Inverse scattering imaging using time-domain ultra-wideband radar," *URSI Radio Science Meeting Digest,* Baltimore, MD.

Two graduate students at the University of Illinois worked on the frequency-domain system project consecutively. Their theses are as follows:

Klemens, G. (1996). "The construction of a device capable of performing microwave tomography and its application," M. S. thesis, University of Illinois, Champaign.

Lee, T. (1997). "A portable automated stepped-frequency radar system used for inverse scattering algorithms," M. S. thesis, University of Illinois, Champaign.

The frequency-domain system from Mr. Lee's thesis is summarized in Appendix B.

Appendix B
Summary of Frequency-Domain System[1]

Introduction

The goal of this system from the beginning was to provide the amplitude and phase of the scattered signal produced by some scatterer. These data would then be processed by one of the many inverse scattering algorithms developed at the University of Illinois to reconstruct an image of the original object. Figures B1 and B2 show the original representation and its image reconstruction of two asymmetrical scatterers processed by diffraction tomography.

It is important to note that this is a frequency-domain system. The same results can be achieved in the time domain as well. Inverse scattering algorithms such as the distorted Born iterative method (DBIM) and the local shape function (LSF) are time-domain algorithms that process time-domain data. Both of these methods are more robust, not constrained to the limitations of diffraction tomography. It is therefore desirable for this stepped-frequency radar (SFR) system to provide time-domain data as well. For this to occur, it is necessary for the SFR system to provide data over multiple frequencies so that time-domain data can be extracted upon an inverse Fourier Transform. The main advantage a time-domain system has over a frequency-domain system is its large operating bandwidth, thus providing more information about the scatterer. A narrow pulse in the time domain is translated to a sinc function with a wide main lobe in the frequency domain. The time-domain system reported here, for example, has an operational bandwidth of 8 to 10 GHz. However, an SFR system has the advantage of a better signal-to-noise ratio (SNR) than its counterpart system in the time domain. Therefore, a broadband SFR system would be much more attractive than a time-domain system. The HP8510 Network Analyzer provides exactly this capability, providing the amplitude and phase from 0.5 to 18 GHz; however, this is much too costly and impractical to use as a field device. The

[1] From Lee, T. (1997). "A portable automated stepped-frequency radar system used for inverse scattering algorithms," M. S. thesis, University of Illinois, Champaign.

ideal field device would be a cost-efficient network analyzer in a small box that is portable to the field.

The original design of this SFR system was based on the design in Figure B3. A signal is transmitted at a high frequency ω_0 and mixed (amplitude modulated) with some low-frequency oscillator signal (or LO signal) ω_{LO}. Therefore, the transmitted signals ideally are two spikes at frequencies $\omega_0 \pm \omega_{LO}$. After amplification and transmission, the signal is mixed again (or demodulated) with the LO signal, thus pushing the sidebands further apart to $\omega_0 \pm 2\,\omega_{LO}$. A signal will also appear at the carrier frequency ω_0. This signal will again be mixed (or demodulated) with a phase-shifted version of the original signal. The signal that will be processed here is at $2\,\omega_0$. The amplitude of this signal is dependent on the phase of the phase shifter. As the phase shifter varies continuously, the amplitude of this signal also varies. When the amplitude becomes a maximum, the phase of the scattered signal has been detected. Thus, coherent detection is used to detect the amplitude and phase of the scattered signal. In actuality, however, this is not really the phase of the scattered signal as phase shift has been introduced from various components such as mixers, amplifiers, power dividers, as well as the background clutter. These effects, however, can be reduced through a deconvolution calibration scheme.

First SFR Design

The system that was first implemented is shown in Figure B3. The operating range of this system is 1 to 2 GHz.

The two major changes from the previous system occur with the source and the phase shifter. A new phase shifter was designed so that it could be controlled via a computer. The source that was originally implemented (YIG-tuned oscillator from Avantek, AV-70502) was not usable because there was excessive frequency drift. Therefore, it was replaced with a highly stable phase-lock loop (PLL) frequency synthesizer. An evaluation kit purchased from Motorola operates from 1,466 to 1,486 MHz. The kit came with a software controlling program called "PLL.EXE" (this is installed in the PC in room 450C of the Electromagnetics Laboratory in the folder "tom - stuff"), which is written in PASCAL language. The board is capable of operating between 0.5 and 2 GHz if the voltage-controlled oscillator (VCO) is changed. The original VCO was replaced with a VCO from Vari-L that operates between 1 and 2 GHz. Software programs to control the data acquisition board had been purchased in the HP VEE language. Therefore, a computer program was written in HP VEE to control the voltage source to make the entire system software consistent. This data acquisition board was purchased from Computer Boards and has two analog outputs, eight analog inputs, and eight digital I/O lines. The two analog outputs were used to control the two voltage-controlled attenuators comprising the phase shifter. Three digital outputs were used to control the digital phase shifter, and three more digital outputs were used to control the source. An analog input was used to detect the amplitude of the scattered signal. Various programs were

written in HP VEE to control the phase shifter, source, and the entire system. (The names of these programs are listed in Mr. Lee's notebook.)

The main problem with this system is the excess data acquisition time. The time it takes for the system to measure the amplitude and phase of the scattered signal for each TX-RX point is roughly 7 min. This is very impractical if one wants to take measurements for several points and especially for many frequencies. The reason for the lengthy time is due to the phase shifter operation. Fifty-three control voltages were applied to achieve a continuous 45-deg phase shift. Thus, for a full 360-deg continuous phase shift, 8×53 control voltages were applied.

Second SFR Design

To reduce the data acquisition time, an in-pulse (I) and quadrature (Q) demodulator is used to detect the amplitude and phase of the scattered signal. Figure B4 (a) shows the design that is used for this current system, and Figure B4 (b) gives a schematic of an I and Q demodulator. This design was used so that we could vary the frequency and always mix the signal down to a fixed frequency (which is 71.3 MHZ in this case). Thus, a narrow-band I and Q demodulator could be purchased and is much more readily available and less costly than a broad-band component. This design still provided some of the advantages from the original design; i.e., it eliminated errors from source leakage.

Basically, an I and Q demodulator splits the incoming signals into in-phase and quadrature components. From this, it is easy to obtain the amplitude and phase of the incoming signals. The most important characteristics of this device are amplitude and phase imbalance. Although one could easily build such a device, there would be a significant amount of imbalance in the amplitude and phase. The advantage of purchasing a completed demodulator is that the mixers and 90-deg phase shifter are specially constructed to minimize these errors.

As with the previous system, the PLL outputs a sinusoidal signal at a designated frequency between 1 and 2 GHz. The power level of each signal varies with frequency; therefore, amplifier Al was added to reduce the fluctuations in power throughout the entire frequency range. The power levels for each frequency are listed at the end of this report. A 9-db attenuator is placed between the PLL and amplifier Al. This was done to prevent the amplifier from oversaturation. Oversaturation is undesirable because the fundamental peak would not be amplified as much, but its harmonics are amplified significantly. The LO has a power level of approximately -8 dbm. There is one correction in the circuit of Figure B4(a). Low-pass filter Ll should be connected at the output of amplifier A2 rather than the input as shown. This provides better spurious suppression than the case drawn here. Attenuators of 6 db and 10 db are attached to the input of the LO and IF ports of mixer Ml because the 1-db compression point of this mixer is 0 dbm. Typically, one wants to operate at several decibels below this point. Amplifiers A3 and A4 are the same 18- to 20-db amplifiers from Macom.

Filter L2 is added to suppress signals greater than 71.3 MHz since that is the frequency that will be processed. A 3-db attenuator is connected at the output of this filter so that the RF port of the I and Q demodulator is operating below its 1-db compression point of 0 dbm. The signal from the 71.3-MHz oscillator, amplified by A5, is fed into the LO port of the demodulator. The LO is further amplified because the LO port of the demodulator requires a 10.5-dbm signal. The I and Q outputs will have signals at DC and at 142.6 MHz. The upper sideband is filtered out, and the DC portion is fed into one of the analog inputs of the data acquisition board.

The components used for this system are labeled in Table B1. This system is controlled through an HP VEE program.

Table B1
Microwave Components for New SFR System

Component	Function	Model No.	Manufacturer
Mixer - M1 Mixer - M2	TX Mixer RX Mixer	MD-140 ZFL-110	Macom Mini-Circuit
Amplifier - A1 Amplifier - A2 Amplifier -A3 Amplifier -A4 Amplifier -A5	Source Amp LO Amp TX Amp 1st RX Amp LO Amp to I and Q Demodulator	AM56-001 ZFL-500N AM56-001 AM56-001 ZFL-500N	Macom Mini-Circuit Macom Macom Mini-Circuit
71.3 MHZ Oscillator Circuit	Local Oscillator (LO)		
PLL Frequency Synthesizer VCO	Source Source	MC145201EVK VCO-110	Motorola Vari-L
2-Way Power Divider - PD1 3-Way Power Divider - PD 2	Source Power Divider LO Power Divider	ZAPD-21 PSC-3-1	Mini-Circuit Mini-Circuit
Low-Pass Filter L1 Low-Pass Filter L2 Low-Pass Filter L3 Low-Pass Filter L4	LO Filter RX Filter I and Q Filter I and Q Filter	SLP-70 SLP-70 SBLP-39 SBLP-39	Mini-Circuit Mini-Circuit Mini-Circuit Mini-Circuit

For this new system, three digital output lines are used for the PLL, and two analog inputs are used to access the I and Q DC voltages. The two analog outputs and the three digital outputs for the analog and digital phase shifters, respectively, were not needed. The data acquisition time for this system is substantially shorter.

Results

This section shows the results of the data taken with three systems: the HP8510 Network Analyzer, the old system design, and the new system design. Figure B5 shows the reconstructed image with the HP Network Analyzer operating at 1.5 GHz. Figure B6 shows the reconstructed image with the old system

operating at 1.0 GHz. Figure B7 shows the reconstructed image with the new system operating at 1.0 GHz. Figure B8 shows the reconstructed image with the new system operating at 1.5 GHz, and Figure B9 shows the reconstructed image with the new system operating at 2.0 GHz. Note that the results for the new system design are much better than the one shown in the thesis. The reason for this is that the phase shifter was slightly improved after the thesis was deposited, thus giving better results. Note that the new system produces results just as well as the old system, but data collection is much faster with the new system.

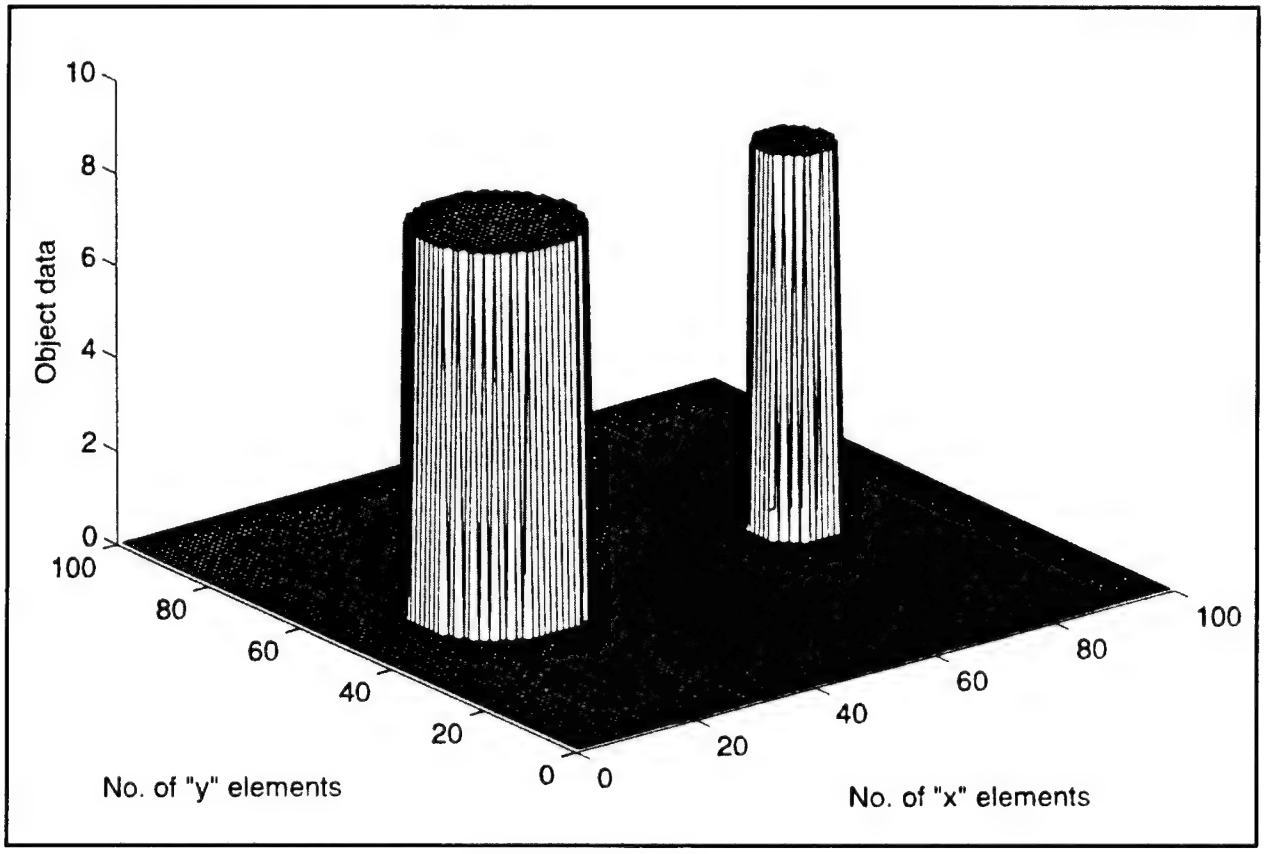

Figure B1. Original representation of two asymmetrical scatterers in 3-D imaging

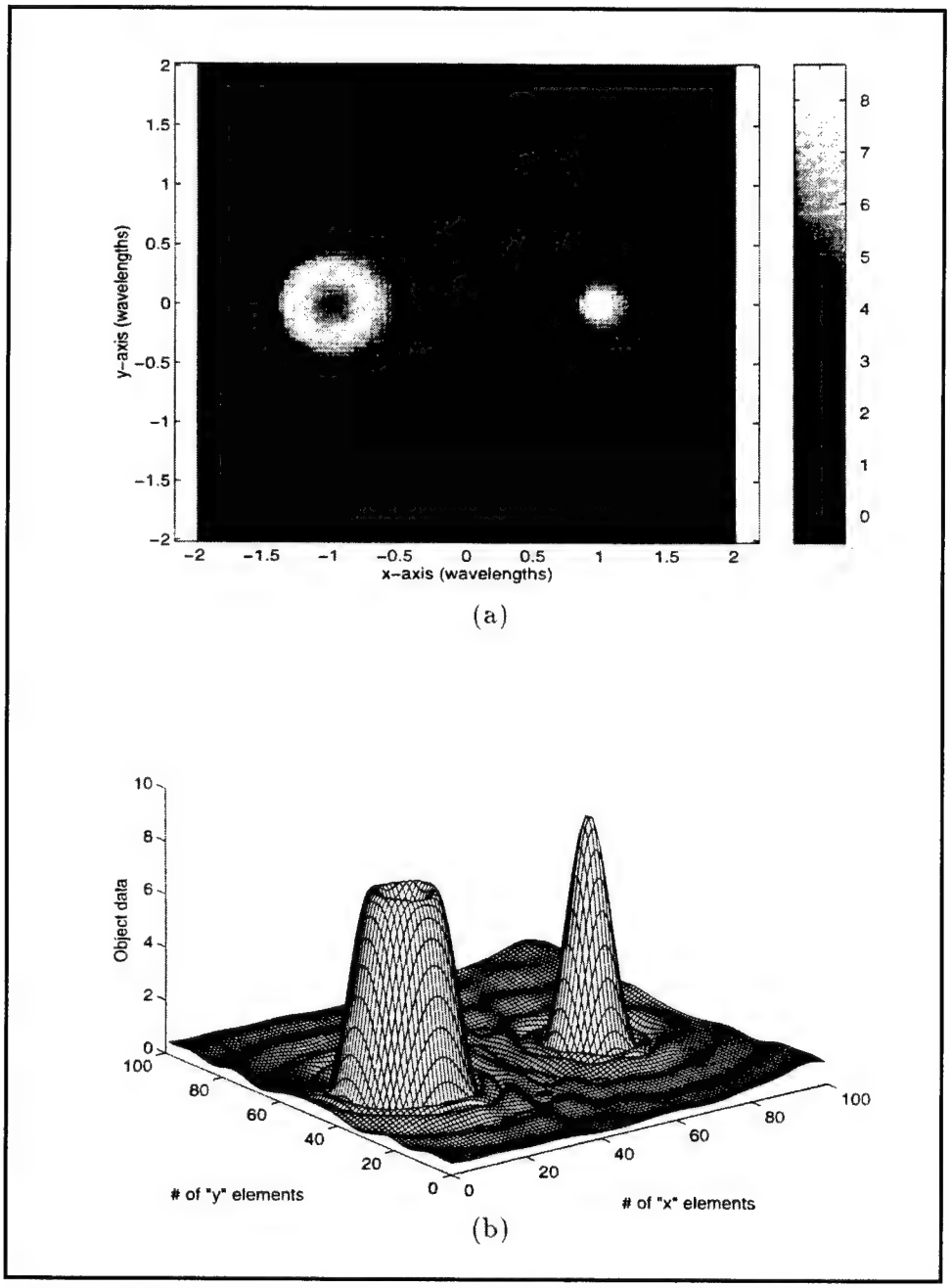

Figure B2. 2-D image (a) and 3-D image (b) of objects in Figure B1 for 25 Rx-Tx points

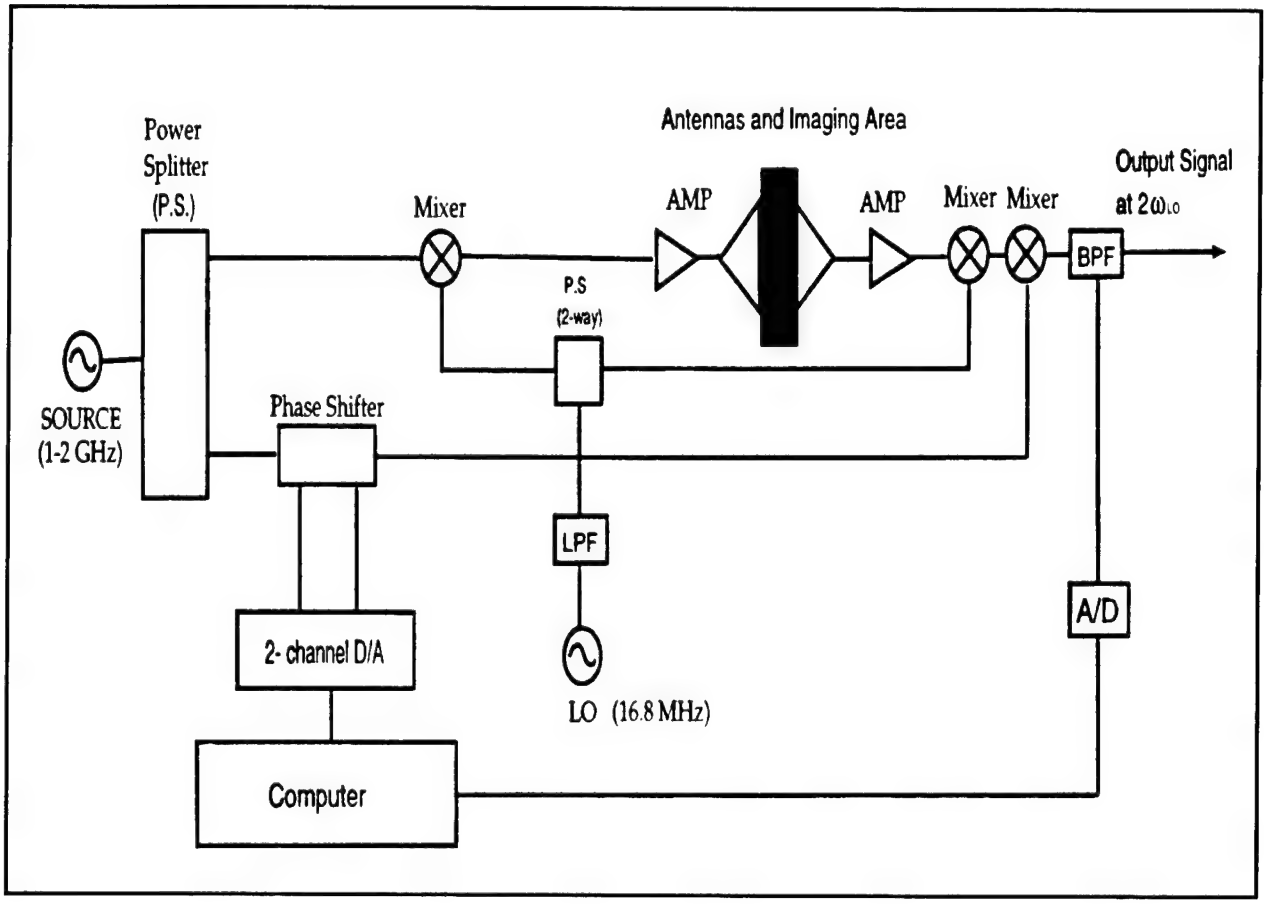

Figure B3. Old SFR system design

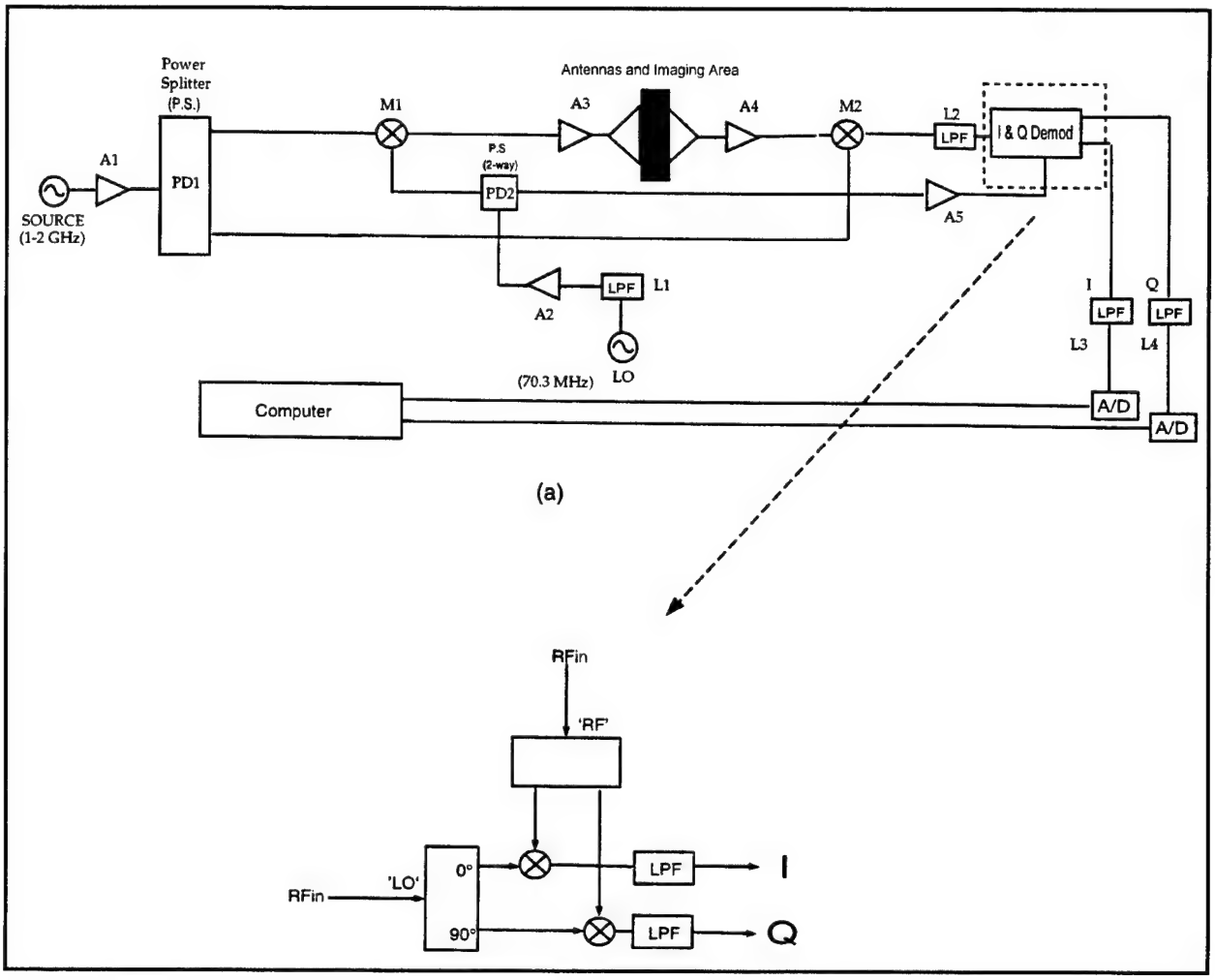

Figure B4. New SFR system design (a) and schematic of I and Q demodulator (b)

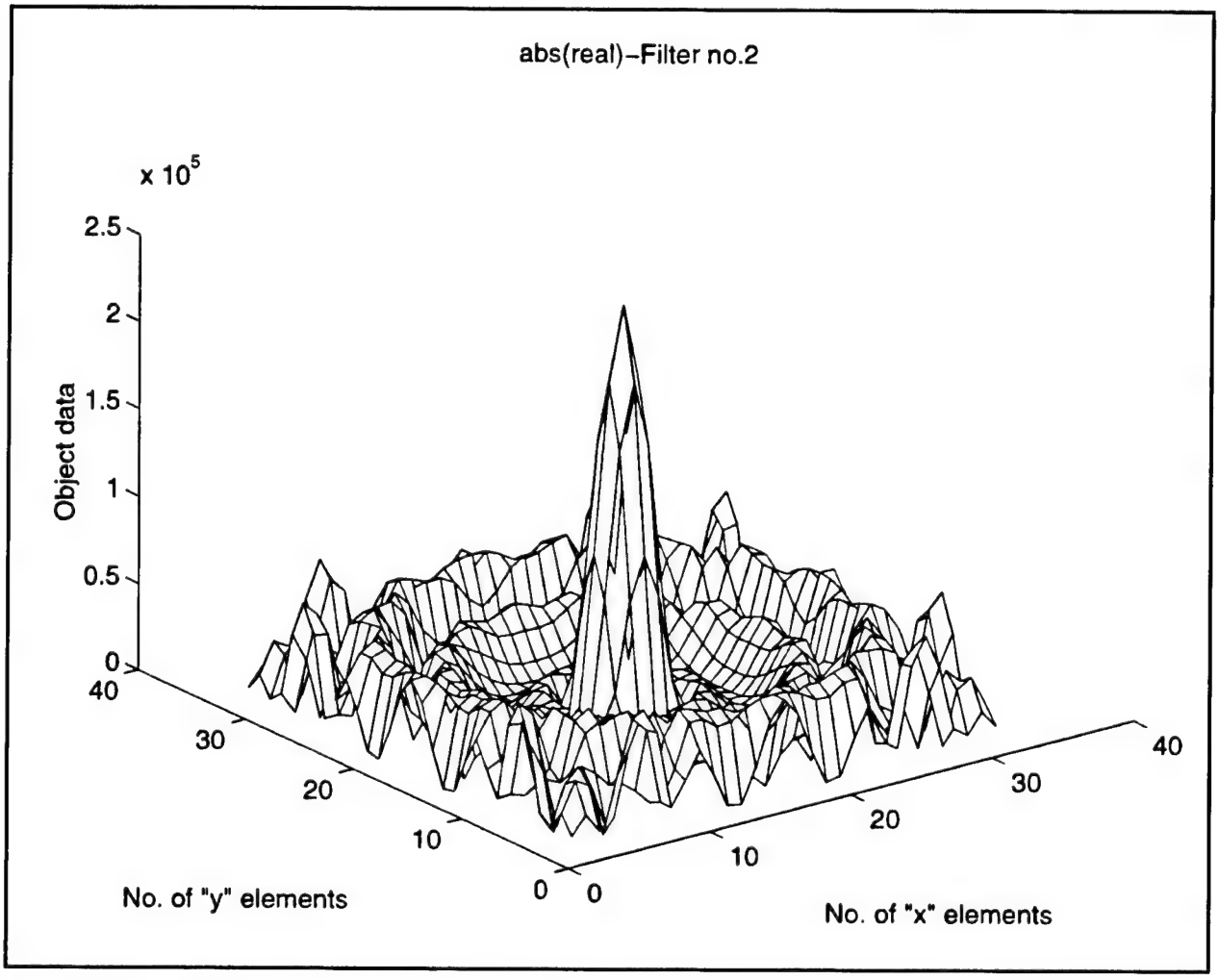

Figure B5. Image with network analyzer at 1.5 GHz

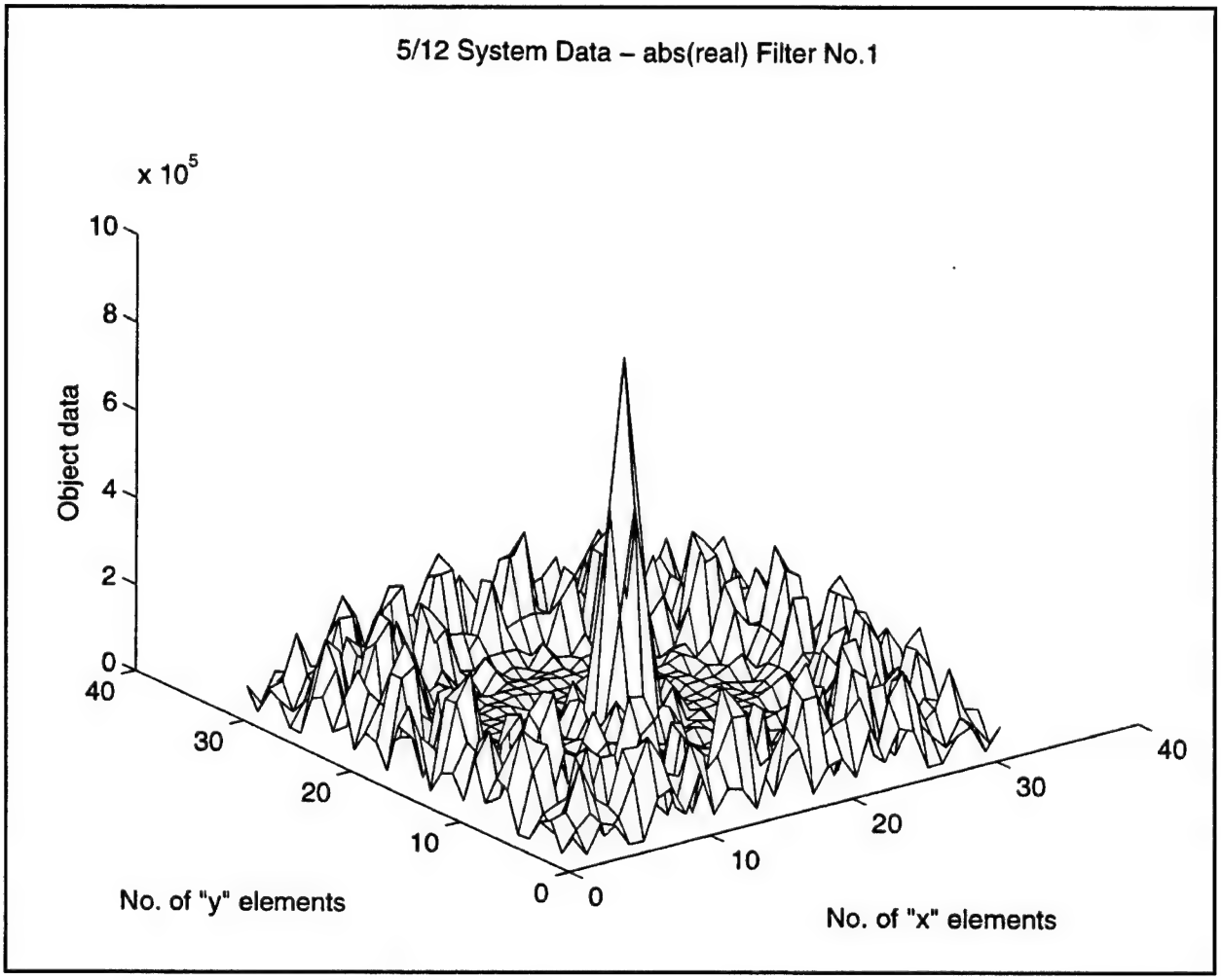

Figure B6. Image with old system at 1.0 GHz

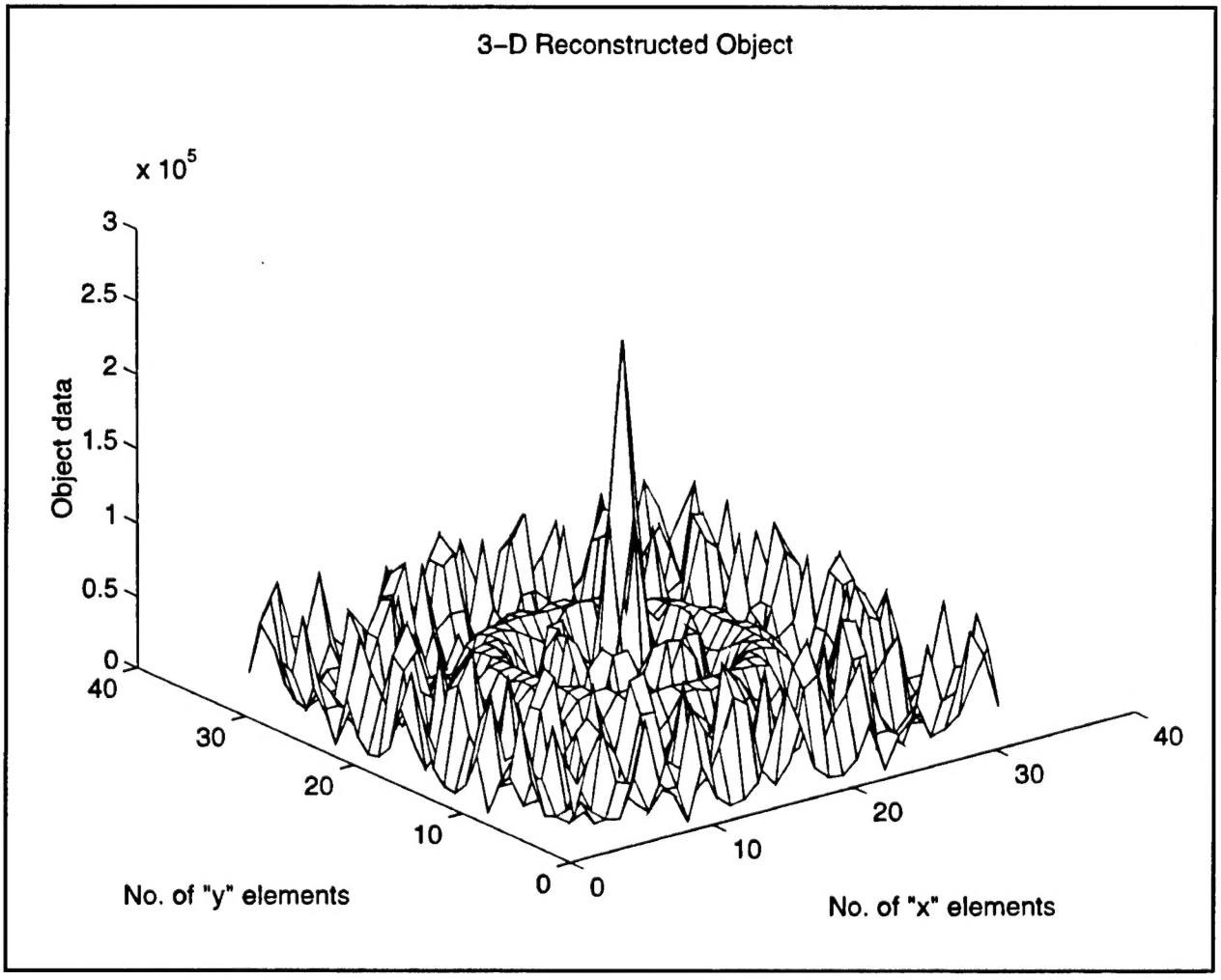

Figure B7. Image with new system at 1.0 GHz

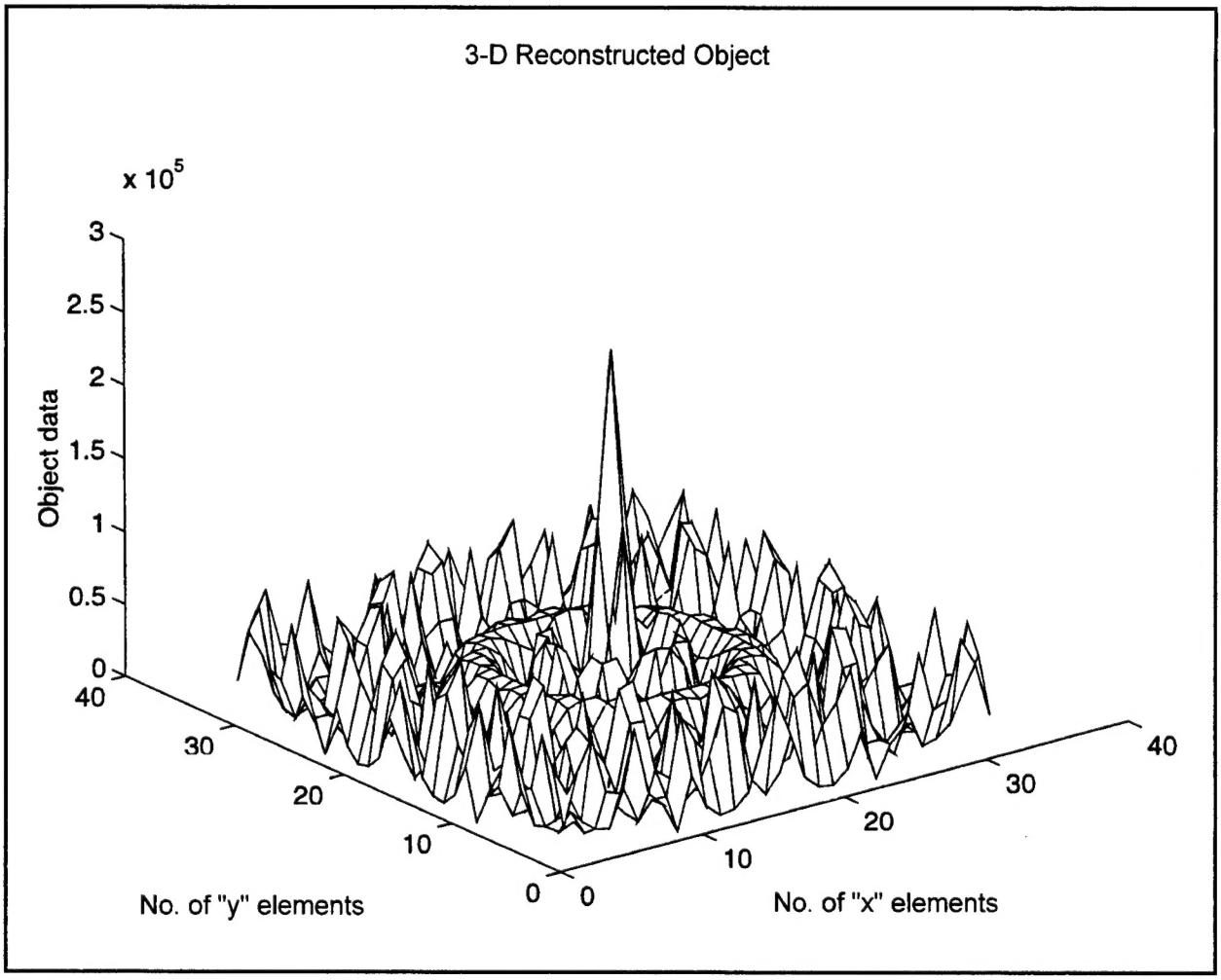

Figure B8. Image with new system at 1.5 GHz

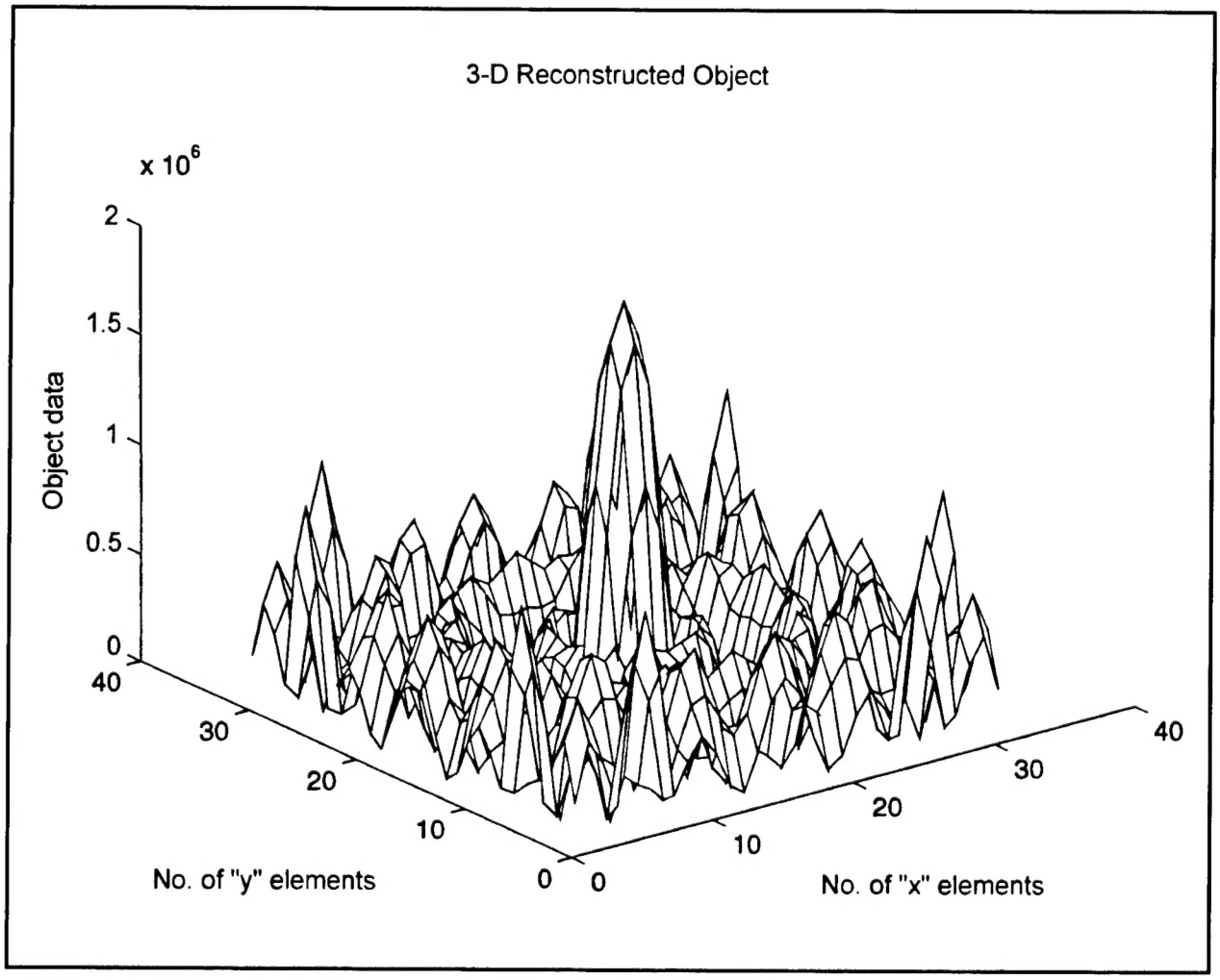

Figure B9. Image with new system at 2.0 GHz

REPORT DOCUMENTATION PAGE

Form Approved
OMB No. 0704-0188

1.AGENCY USE ONLY *(Leave blank)*	2.REPORT DATE	3.REPORT TYPE AND DATES COVERED
	June 1998	Final report

4.TITLE AND SUBTITLE
A Portable, Nondestructive Evaluation System

5.FUNDING NUMBERS

6.AUTHOR(S)
Fu-Chiarng Chen, Weng Cho Chew, A. Michel Alexander

7.PERFORMING ORGANIZATION NAME(S) AND ADDRESS(ES)
Department of Electrical and Computer Engineering, University of Illinois;
1406 West Green, Urbana, IL 61801;
U.S. Army Engineer Waterways Experiment Station, 3909 Halls Ferry Road,
Vicksburg, MS 39180-6199

8.PERFORMING ORGANIZATION REPORT NUMBER
Technical Report CPAR-SL-98-2

9.SPONSORING/MONITORING AGENCY NAME(S) AND ADDRESS(ES)
U.S. Army Corps of Engineers
Washington, DC 20314-1000

10.SPONSORING/MONITORING AGENCY REPORT NUMBER

11.SUPPLEMENTARY NOTES
Available from National Technical Information Service, 5285 Port Royal Road, Springfield, VA 22161.

12a.DISTRIBUTION/AVAILABILITY STATEMENT
Approved for public release; distribution is unlimited.

12b.DISTRIBUTION CODE

13.ABSTRACT ***(Maximum 200 words)***

This project was a cooperative effort between the U.S. Army Engineer Waterways Experiment Station (WES) and the University of Illinois under a Cooperative Research and Development Agreement as part of the Construction Productivity Advancement Research Program. The purpose was to develop a portable radar system for nondestructive evaluation (NDE) of concrete. Two approaches, a time-domain pulse system and a frequency-domain system, were investigated. An ultra-wideband (UWB) time-domain pulse radar NDE system was developed at the University of Illinois and field tested at WES. The UWB time-domain impulse radar system successfully demonstrated the capability of detecting small reinforcement bars embedded in large concrete blocks. This report describes the development of the UWB time-domain NDE system in detail and illustrates several experimental results.

14.SUBJECT TERMS
Concrete evaluation
Nondestructive evaluation system
Portable radar system
Ultra-wide-band time-domain pulse radar system

15.NUMBER OF PAGES
57

16.PRICE CODE

17.SECURITY CLASSIFICATION OF REPORT	18.SECURITY CLASSIFICATION OF THIS PAGE	19.SECURITY CLASSIFICATION OF ABSTRACT	20.LIMITATION OF ABSTRACT
UNCLASSIFIED	UNCLASSIFIED		